Development of a Simulation Process for Conceptual CS-23 Propeller Aircraft System Noise Assessment

Hon, K.S.; Domogalla, Vincent ; Feldhusen-Hoffmann, Antje ; Blinstrub, J.; Bertsch, Lothar; Snellen, M.; Zill, Thomas ; Angermann, Maik

DOI
10.2514/6.2025-3365

Publication date
2025

Document Version
Final published version

Published in
AIAA aviation forum and ASCEND 2025

AIAA Aviation Forum and ASCEND co-located Conference Proceedings
21 - 25 July 2025, Las Vegas, Nevada
AIAA AVIATION FORUM AND ASCEND 2025

10.2514/6.2025-3365

Development of a Simulation Process for Conceptual CS-23 Propeller Aircraft System Noise Assessment

Kai San Hon *[1], Vincent Domogalla †[2], Antje Feldhusen-Hoffmann ‡[1], Jason Blinstrub §[2], Lothar Bertsch ¶[2], Mirjam Snellen ‖[4], Thomas Zill **[3], and Maik Angermann ††[3]

[1]*German Aerospace Center (DLR), 52146 Würselen, Germany*
[2]*German Aerospace Center (DLR), 37073 Göttingen, Germany*
[3]*German Aerospace Center (DLR), 21129 Hamburg, Germany*
[4]*Delft University of Technology, 2629 HS Delft, Netherlands*
[5]*Technical University of Braunschweig, 38108 Braunschweig, Germany*

Many highly interdependent disciplines are concerned with the system noise assessment of small propeller aircraft concepts, including aircraft, propeller, engine design and acoustic modelling, flight trajectories calculation, noise propagation and ground effect modelling. There are no state-of-the-art simulation processes in Europe which account for all the aforementioned disciplines, as efforts heretofore have been focused on large transport aircraft concepts. This paper presents the development of such a simulation process at the German Aerospace Center (DLR). The simulation process inputs top-level aircraft design requirements, producing a valid CS-23 conceptual propeller aircraft design. It then calculates realistic flight paths for departure and approach for the conceptual aircraft and simulates noise immissions at user-specified locations. The immissions assessment would then guide design modifications, low-noise flight trajectory generation and novel aircraft design. A Reims-Cessna F406 is considered as the reference aircraft and is used to obtain the first results from the simulation process. The results are compared with measurements from a flight test campaign using the same aircraft. Important effects observed in the results and in the immissions assessments are also presented in this paper. Furthermore, the capabilities of the simulation chain will be demonstrated with sensitivity studies that show the effects of modifying operational procedures on ground noise immissions.

Keywords: Aircraft Design, Aircraft Noise, Aircraft Noise Measurements

I. Nomenclature

AGL	=	Above Ground Level
β	=	Propeller blade pitch
C_P	=	Coefficient of power (Propeller)
C_T	=	Coefficient of thrust (Propeller)
DLR	=	German Aerospace Center
δ_f	=	Flap deflection angle
EASA	=	European Union Aviation Safety Agency
EM	=	Aircraft empty mass
EPNL	=	Effective perceived noise level
η	=	Propeller efficiency
FAR	=	Federal Aviation Regulations

*Doctoral Researcher, Institute of Aerodynamics and Flow Technology, Carlo-Schmid-Straße 12.
†Doctoral Researcher, Institute of Aerodynamics and Flow Technology, Bunsenstrasse 10.
‡Research Scientist, Institute of Aerodynamics and Flow Technology, Carlo-Schmid-Straße 12.
§Research Scientist, Institute of Aerodynamics and Flow Technology, Bunsenstrasse 10.
¶Research Scientist, Institute of Aerodynamics and Flow Technology, Bunsenstrasse 10.
‖Professor of Acoustic Data Analysis and Imaging for Aviation Noise, Faculty of Aerospace Engineering, Kluyverweg 1.
**Research Scientist, Institute of System Architectures in Aeronautics, Hein-Saß-Weg 22.
††Research Associate, Institute of Flight Guidance, Hermann-Blenk-Straße 27.

γ	=	Climb angle
IAS	=	Indicated air speed
ICAO	=	International Civil Aviation Organization
J	=	Advance ratio
KIAS	=	Knots of Indicated Air Speed
KTAS	=	Knots of True Air Speed
L	=	Sound pressure level
L_A	=	A-weighted sound pressure level
LTO	=	Landing & Take-Off
MFM	=	Aircraft maximum fuel mass
MLM	=	Aircraft maximum landing mass
MRM	=	Aircraft maximum ramp mass
MTOM	=	Aircraft maximum take-off mass
MZFM	=	Aircraft maximum zero fuel mass
n	=	Propeller rotational speed
SEL	=	A-weighted sound exposure level
t	=	Engine torque
θ	=	Aircraft pitch angle
TAS	=	True air speed

II. Introduction

A. Low-Noise Aircraft Design

The Strategic Research and Innovation Agenda of the European Union Clean Aviation Joint Undertaking envisages the use of small aircraft in regional and inter-urban mobility of people and goods in the European Union, especially over distances of less than 500 km, by mid-2030 [1]. This is because regional aircraft are considered the first area where innovative and disruptive technologies for the reduction of the environmental footprint of aviation, such as hybrid and electric propulsion technologies, can be applied. However, increased usage of small aircraft in urban areas and urban airports comes with increased noise immissions for communities or urban areas around such airports [2]. Therefore, it is of interest to research the noise impact of small aircraft flying close to communities at low altitudes, i.e. during approach and departure, leading to an increasing emphasis on using ground immissions as a design objective during conceptual aircraft design.

Examples of initiatives that emphasize ground noise immissions as an aircraft design objective include the silent aircraft initiative [3] by the University of Cambridge and the Massachusetts Institute of Technology (MIT) that investigates the use of alternative flight operations for noise reduction around airports and the design of the novel low-noise and fuel efficient SAX-40 conceptual aircraft. Another example is the European Union Clean Aviation Joint Undertaking [1], which sets out a road map and lists the key technologies with the aim to reduce future aircraft emissions for Europe. Such initiatives also exist at the national level in Europe. For example, low-noise aircraft design activities have begun as early as 2008, where the DLR Institute of Aerodynamics and Flow Technology and the Institute of Aircraft Design and Lightweight Structures at Technical University of Braunschweig (TU Braunschweig) joined forces to link noise prediction capabilities from the DLR with the aircraft design competencies at the TU Braunschweig, with the aim to develop a simulation process for low-noise aircraft design [4, 5, 6, 7].

B. Aircraft System Noise Modelling

Accurate modelling of aircraft system noise is essential when using ground noise immissions as a design objective. Aircraft system noise is defined as the noise received or detected on the ground, considering not only the noise emission from various aircraft noise sources but also atmospheric effects during noise propagation, and ground effects on the received signal [8]. The contribution of each source varies with aircraft configuration (i.e. clean configuration versus configurations with high-lift devices deployed) and operating condition (i.e. different procedures adopted during approach or departure). Parametric noise source modelling is essential to adequately capture these effects. Aircraft noise is modelled by considering the contributions from important sources, and much research has been conducted in

the development of parametric noise models for specific aircraft components or noise sources.

For this purpose, many simulation tools are developed for predicting aircraft system noise in different research institutions around the world. Examples include the Parametric Aircraft Noise Analysis Module (PANAM) [5] from DLR, Aircraft Noise Prediction Program (ANOPP) [9] from the National Aeronautics and Space Administration (NASA) of the United States of America, Codes Acoustiques par Rayons pour la Modélisation et l'Estimation de Nuisances (CARMEN) [10] from the Office national d'études et de recherches aérospatiales (ONERA) of France and the Aircraft Noise Estimation Tool (AiNEST) [11] from the Japan Aerospace Exploration Agency (JAXA). These tools are commonly component-based (i.e. taking into account the contribution of noise sources from various aircraft components), parametric (i.e. requiring the inputs of various parameters crucial to conceptual aircraft design, e.g. aircraft geometry) and emission-based (i.e. considering the noise emission at the sources, and then propagating the noise to user-defined observers). They also typically employ semi-empirical or analytical noise prediction models to avoid long and costly computations, although they can also interface to high-fidelity test data or simulation benchmarks.

However, an aircraft noise prediction tool itself is not sufficient for overall aircraft noise assessment. Many disciplines are concerned with aircraft noise assessment, namely aircraft, engine, propeller design, aircraft performance and flight trajectories calculation, noise propagation and ground effect modelling. Therefore, to perform an overall aircraft noise assessment, a simulation process that accounts for all the aforementioned disciplines is necessary.

C. State-of-the-Art & Project Goals

Although simulation processes that produce detailed assessments of noise immissions for large turbofan-driven transport aircraft concepts already exist and are largely well-tested, at the time of writing, there are no state-of-the-art simulation processes that include aircraft design, trajectory generation and produce a noise assessment for a small propeller-driven aircraft, namely those commonly used in general and regional aviation, to the best of the authors' knowledge. Noise of small propeller-driven aircraft has been previously investigated, but only at a very low level of fidelity (fully empirical and not accounting for all disciplines) or only limited to single operating conditions and directly at the source (aeroacoustic simulations or component measurements) [12]. Moreover, noise and local gaseous emissions and immissions were treated separately in all known research activities, and no process for the overall assessment of the two is currently available [4, 13, 14].

Project L^2INK [15] (*Lärm und Lokale Schadstoffe im Innovationszentrum für Kleinflugzeug-Technologien*, or Noise and Local Pollutants at the Innovation Center for Small Aircraft Technologies) is therefore established with the aim to link up the fields of research, simulation tools and experts surrounding noise and local gaseous emissions. The goal is to establish a multidisciplinary simulation process to calculate noise and local gaseous immissions of EASA CS-23 (generally considered to be equivalent to FAR Part 23 airworthiness standards) propeller-driven aircraft.

This paper presents the progress of the realization of the simulation process, and the current capabilities of the simulation process to perform system noise assessment for small propeller aircraft. The tools and methods used is presented in section III.A. The simulation process is then used to design the reference aircraft, a Reims-Cessna F406, as detailed in section IV.A, and to validate its performance as detailed in section IV.B. Noise immissions are then calculated for the F406 and compared with measurements obtained from flyover measurements of the same aircraft in section V. Lastly, sensitivities of the noise immissions to procedural modifications are shown by comparing the results by varying the take-off weight, climb speed and climb power in section V. An in-depth validation of the simulation results in noise immissions is beyond the scope of this paper. This is because, the development of the simulation process and detailed propeller aircraft noise assessment are topics of ongoing research, and thus the noise assessment presented is limited to the key sources, and effects such as propeller broadband noise, installation effects and interaction effects are not completely accounted for. This will be further discussed in this paper.

III. Tools & Methods

A. Simulation Architecture & Tools Used

The simulation process as described in this paper is realized in project L^{2}INK. It starts with top-level aircraft design requirements (TLARs), engine and propeller data, and produces a valid CS-23 aircraft design. The aircraft is then simulated conducting approaches and departures with user-defined procedures using aerodynamic and engine information extracted from the aircraft design, or alternatively can take user-inputted flight paths and performance data. Noise immissions will hence be calculated for these flight paths. Since all aforementioned results will be produced from one unified, fast and cost-efficient simulation process, the user can quickly iterate through preliminary aircraft designs or immissions reduction measures, assess the noise immissions of the aircraft (e.g. whether it complies with certification guidelines), and thereby guide design decisions. An illustration of the simulation process is shown in 1.

The tools are integrated using the Remote Component Environment (RCE) [16], and exchange data with each other using the Common Parametric Aircraft Configuration Schema (CPACS) [17], which describes air transport vehicle characteristics, such as airframe geometry, engine performance and mission profiles in an XML file format. The tools and methods employed in the simulation process are explained in more detail in the sections III.A.1, III.A.2, III.A.3 and III.B. Together, they realize the core functionality of the simulation process, enabling the present work, and is essential for the next steps in the identification of gaps in existing knowledge and capabilities. New insights from project L^{2}INK will also be integrated into the simulation process as capabilities expand [18, 19].

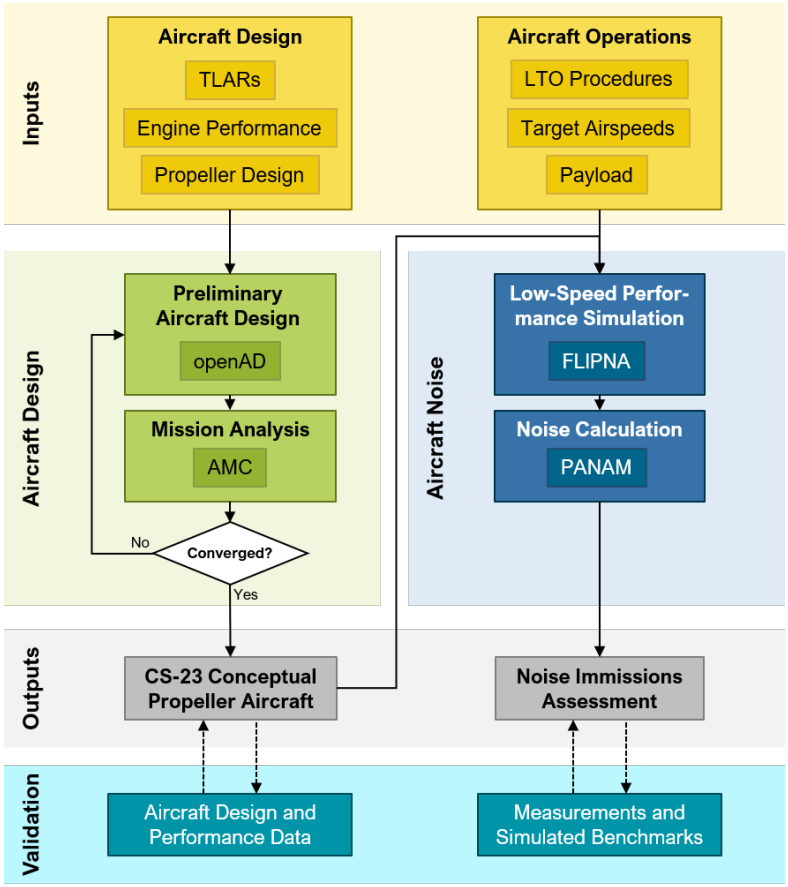

Fig. 1 Illustration of the simulation process architecture.

1. Aircraft Design & Mission Performance Calculation

openAD [20] is a python-based multi-disciplinary and multi-fidelity preliminary aircraft design tool. This tool uses established methodologies from publicly available handbooks or custom solutions for disciplines where adequate methods were not readily found in the literature. It can process TLARs stored in CPACS format and generate valid conceptual aircraft designs, which are then exported to a CPACS output file. The CS-23 aircraft design capabilities of openAD are currently under development, and is used to recreate the reference aircraft digitally for this work..

Aircraft Mission Calculator (AMC) [20] is a tool used to estimate the mission performance of conceptual aircraft. AMC computes an aero-engine performance optimized step climb and also performs initial cruise altitude optimization and trim drag calculation at each time or mass step. AMC is used in the simulation process to calculate and validate the mission performance of the reference aircraft design using the user-inputted detailed engine data.

2. Low-Speed Performance Calculation

FlightPaths for Noise Analysis (FLIPNA) [6] calculates trajectories for take-off and landing from procedural profiles based on ECAC Doc 29 [21] using the detailed aerodynamics and engine performance from the aircraft design. Additionally, it can also generate procedural profiles, where users can define specific inputs for approach and departure procedures such as the altitudes of selected climb or acceleration segments, calibrated air speeds at the end points of said segments and throttle ratings for take-off and after cutback. Furthermore, PANAM can directly read the outputs of FLIPNA to perform noise simulations. FLIPNA is well-tested for conventional large transport aircraft with turbofan engines [6], and has been adapted for propeller aircraft for this project.

3. Aircraft Noise Calculation

Parametric Aircraft Noise Analysis Module (PANAM) [5] simulates aircraft noise emission and transmission for conceptual aircraft designs. PANAM predicts the ground noise impact for single flyover events by considering the contribution of individual aircraft noise sources for emissions analysis, and atmospheric propagation effects and ground attenuation effects at user-specified ground observers for transmission and immission analysis. Additionally, PANAM can use external source inputs from different tools and assess uncertainties of the results. Example sources and methods applied in the model used for this study include airframe noise sources (leading, trailing edge high-lift devices and landing gear) which implement models as described in [5, 22, 23, 24, 25, 26], as well as various sound propagation (e.g. SAE ARP866A [27], ISO 9613 [28]) and ground attenuation models (e.g. Chien-Soroka [29]).

Similar to FLIPNA, PANAM is well-tested for conventional transport aircraft mounted with turbofan engines [30] and is extended to propeller aircraft using Hanson's propeller noise models [31, 32], more on this in section III.B.

B. Modelling of Propeller Noise in PANAM

The most important feature of the propeller noise model is the ability to provide predictions with reasonable accuracy and low computation times. It should also cover the effect of all relevant parameters influencing the noise impact on the ground. In general, this leaves empirical methods like the SAE AIR 1407 model [33], or methods with a predefined solution of the wave equation, like Farassat's solutions (esp. equation 1A) [34] and the Hanson propeller model [31]. Empirical propeller noise models have the advantage that they can also include broadband noise without further computational effort. However, this limits their use to cases aligned with those used for establishing the model. Modelling broadband noise is also possible with the Hanson and Farassat models, but this requires an unsteady flow solution. For the tonal part, Hanson's helicoidal surface theory requires the blade geometry and radial lift and drag coefficients as input, which are obtainable from, for example, blade element methods (BEM). Farassat's equation 1A requires surface pressure as input and is usually coupled with 3D aerodynamic solvers, e.g. 3D panel methods [18]. Compared to the 2D BEM methods, the 3D solution of the propeller flow is much more computationally intensive.

Based on the findings of Hanson [32], Hubbard [35], and Akiwate [36], broadband noise is negligible for isolated propellers with low tip mach numbers and less than 6-8 blades. Coupled with the low computational effort for the flow solution, the Hanson model is therefore considered the most appropriate method for the current application.

IV. Modelling of Reference Aircraft in the Simulation Process

The reference aircraft of project L^{2}INK, the Reims-Cessna F406 Caravan II (F406), is digitally redesigned and validated in this section. The noise immissions are then simulated and compared with data obtained from a measurement campaign in summer 2023. D-ILAB, as shown in figure 2a, performed multiple flyovers at different air speeds and configurations, and its ground noise immissions were measured. More details on the measuurement campaign can be found in Section IV.C.1.

(a) D-ILAB in flight [37]. **(b) F406 digital reference, illustrated in TiGL viewer [38].**

Fig. 2 The Reims-Cessna F406, reference aircraft of Project L^{2}INK.

A. Validation of Design & Mission Performance

D-ILAB was designed in openAD by matching the aircraft geometry [39, 40] and available component weight data [41]. Based on this, openAD calculates the overall aircraft weights and generates the aerodynamic performance maps of the aircraft for clean, departure and approach configurations. In addition, accurate data of the aircraft powerplant, the Pratt & Whitney Canada PT6A-112 turboprop engine (PT6A-112), each supplying a maximum take-off and continuous power of 373 kW [42], is provided by GasTurb GmbH [43]. This includes data such as specific fuel consumption and shaft power over various altitudes and mach numbers. Complementing this are the propeller performance maps of the 5-bladed MT-Propeller MTV-27/220. C_T and η over C_P and J at various altitudes are provided by the manufacturer [44]. Examples of the input parameters and TLARs used in the design are shown in Table 2a. Calibration factors were further applied to the aircraft drag and undocumented component weights while iterating on the aircraft design.

The aircraft design of the F406 is validated by the comparison of various overall aircraft weight, field performance metrics and payload-range diagrams calculated from openAD and AMC, with those found in the the EASA type certificate data sheets [42, 45] and derived from the aircraft information manual (or pilot's operating handbook, POH) [40]. The design is shown in figure 2b, whereas the results are shown in tables 2b and 2c and figure 3. The overall aircraft weights match that of the reference. The payload and range diagram displays a close fit, with points A, B and C deviating no more than 5% in range. Furthermore, the take-off and landing field lengths also do not differ by more than 5%, which is acceptable in preliminary aircraft design.

B. Validation of Low-Speed Performance

Since the approach and departure, i.e. the low-speed flight phases, are the most relevant for noise, it is essential that the low-speed performance of the digital F406 is valid as well. The low-speed aircraft performance of the F406 is validated by comparing aircraft performance data calculated by FLIPNA to that of a real approach and departure. The aircraft performance data are recorded from D-ILAB while performance an approach and departure from Braunschweig-Wolfsburg Airport (ICAO: EDVE). LTO procedures, altitude profile and air speeds are configured in FLIPNA to match that of the real approach and departure as close as possible. The pitch and the thrust required to fly the flight path is then calculated by FLIPNA, and by comparing the two to that recorded in the real flight, the accuracy

Table 2 openAD/AMC input parameters used, and comparisons between the openAD results of the digital design to the reference aircraft [39, 40, 41, 42, 45].

(a) Example input parameters and TLARs used for openAD/AMC.

Metric	Value	Unit	Source
Wing Root / Tip Airfoil	NACA 23018 / 23012	-	[39]
Wing Twist	-3	deg	[39]
Wing Area	23.48	m^2	[40]
Wing Span	15.08	m	[40]
Wing Group Mass	396	kg	[41]
Empennage Group Mass	116	kg	[41]
PT6A-112 Max. (Continuous) Power	373	kW	[45]
PT6A-112 Mass (Dry)	156	kg	[45]
MTV-27/220 Weight	68.2	kg	[44]
Cruise Altitude	10,000	ft	[40]
Cruise Speed	180	KTAS	[40]
$C_{L_{max}}$ in Clean / Landing Configuration	1.23 / 1.94	-	[40]

(b) Aircraft weights.

Mass	Ref. [42] [kg]	openAD [kg]
MRM	4280	4280
MTOM & MLM	4246	4246
MZFM	3856	3856

(c) Field performance (at MTOM & MLM respectively).

Field Length	Ref. [40] [m]	openAD [m]	Delta [%]
Take-Off	803	838	4.36
Landing	757	784	3.57

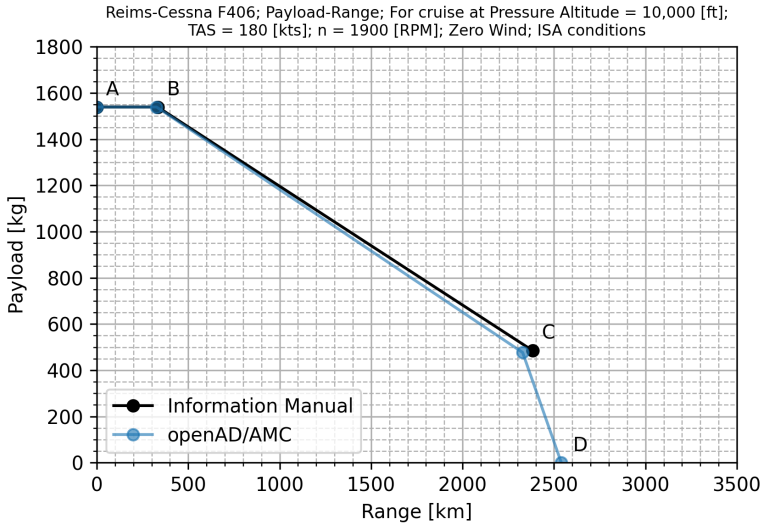

Fig. 3 Comparison of payload-range diagram*.

* The ferry range (point D) of the F406 cannot be found in the information manual, therefore point D cannot be validated.

of the aerodynamic data from openAD and the inputted engine data in low-speed flight can be judged.

The results are shown in figure 4. Results show that there is a satisfactory fit in aircraft pitch and engine thrust

when the aircraft is in a clean configuration, i.e. during the climb after take-off in figure 4b and the early stages of the approach in figure 4a. This proves that the engine and the clean-configuration aerodynamic performance data accurately reflects that of the F406. The accuracy of the results decrease once the flaps are deployed, as shown in figure 4a, which is most likely a result of the aerodynamic effects of the flaps not being as accurately modelled.

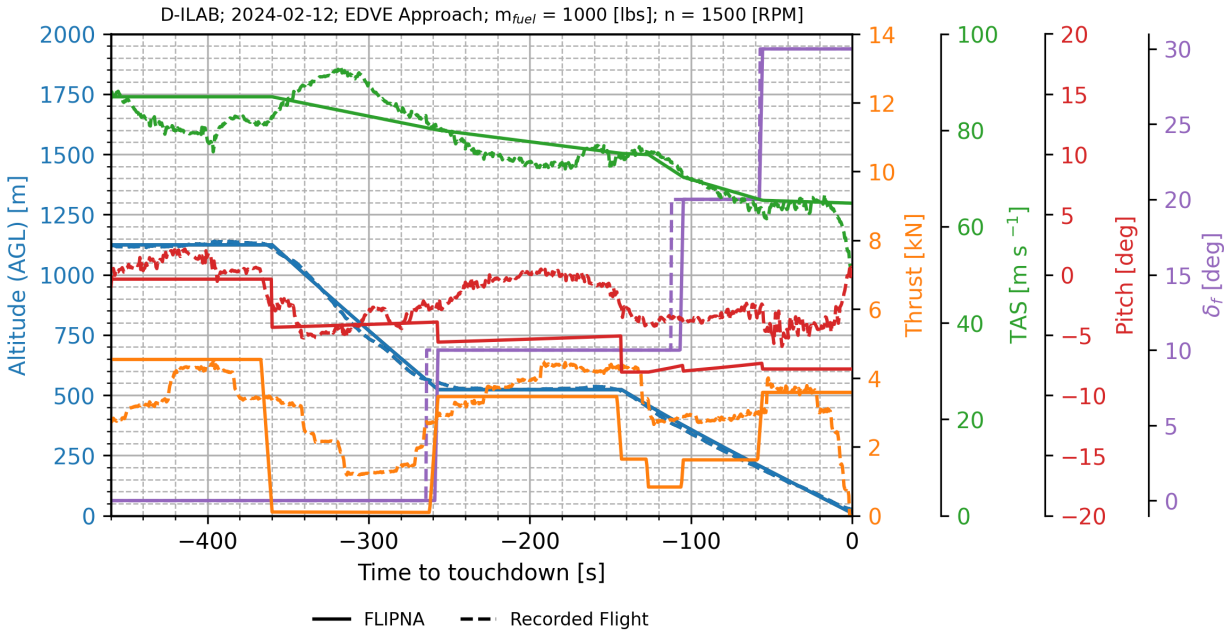

(a) Approach from EDVE.

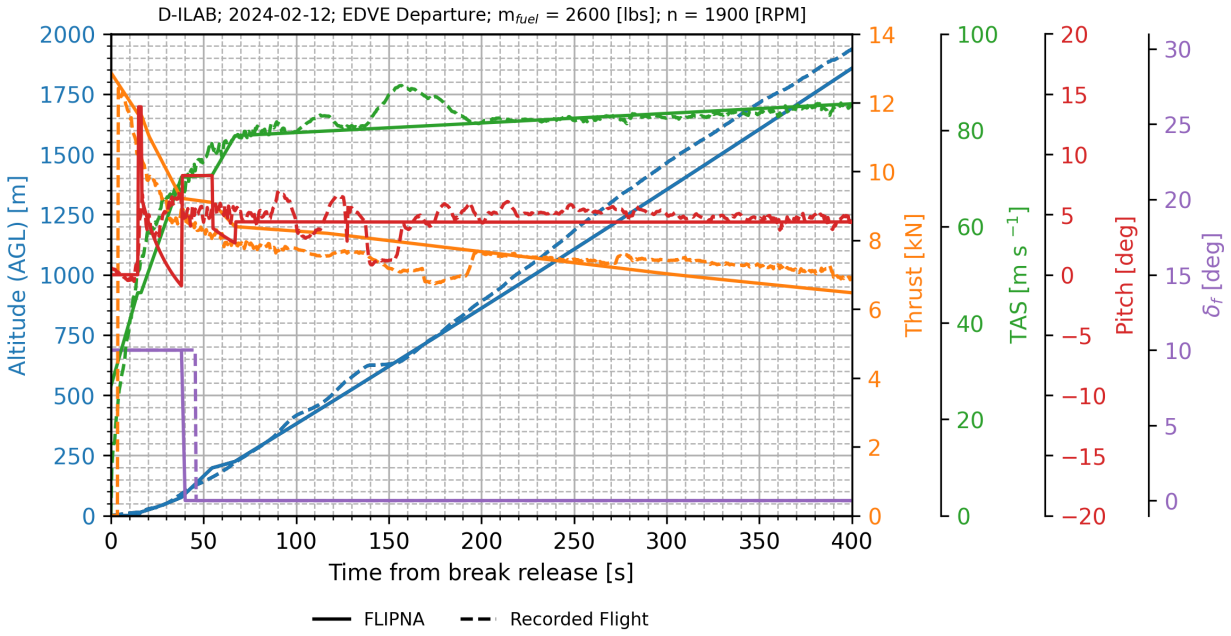

(b) Departure from EDVE.

Fig. 4 F406 low-speed performance validation.

C. Modelling & Comparison of Noise Immissions Results

After assessing the validity of the design and low-speed performance of the F406, the noise calculation and immissions assessment of the F406 can be carried out. To assess the accuracy of the noise modelling, data from flyover measurements are compared with results calculated by the simulation process in this section.

1. Overview of Noise Measurement Campaign

The flight test campaign was conducted between 21 June and 29 June 2023, at Magdeburg-Cochstedt Airport (ICAO: EDBC). The acoustic measurement setup comprises of free field $\frac{1}{2}$-inch condenser microphones installed at six stations, located at the runway safety area as depicted in figure 5. At each station one microphone was installed on a ground plate, on a 1.20 m tripod. Microphones are also mounted on a 6.0 m mast at all stations except that on the runway due to safety reasons, making a total of 14 microphones. The microphone signals are acquired with a sampling frequency of 48 kHz. The measurement uncertainty of the hardware is within ± 1.0 dB, but might deviate to higher values due to surrounding conditions fluctuations. For example, when measuring at wind speeds exceeding 5 kts, the measured value may vary up to ± 2.0 dB from the actual value [15].

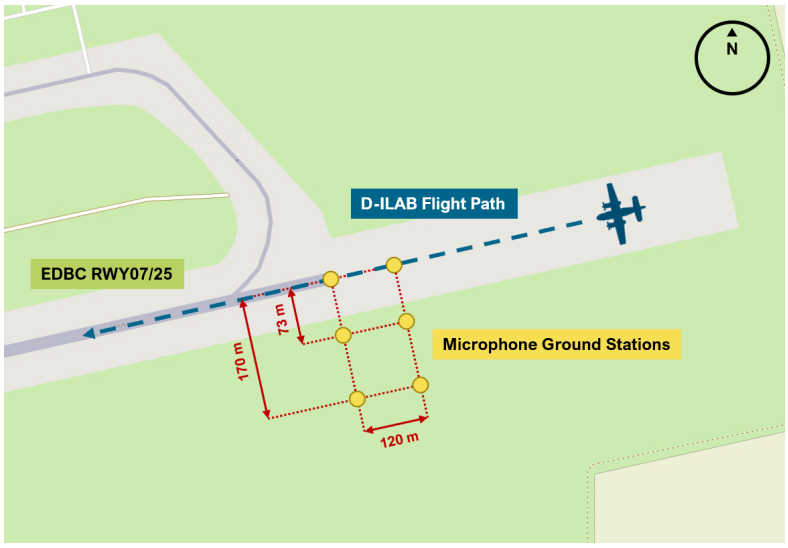

Fig. 5 Illustration of the experiment setup at EDBC (Not to scale) [46].

Table 3 Test matrix of D-ILAB.

Parameters	Tested Quantities
Altitude (Target) [ft AGL]	500
IAS (Target) [KIAS]	130, 145, 160
Gear setting	Up, Down
δ_f [deg]	0, 20
n [RPM]	1600, 1900

The test matrix of D-ILAB is presented in table 3. The altitude, IAS and aircraft configuration is kept constant for 2 km before and after flying over the microphone stations. Each point in the test matrix has been flown three times throughout the campaign. The aircraft performance data is recorded and processed by the test flight team from the Institute of Flight Guidance from TU Braunschweig [37], whereas the measured noise data is gathered and processed by a team at the department of technical acoustics of the DLR Institute of Aerodynamics and Flow Technology.

A total of 65 recordings were made for D-ILAB. For the sake of brevity, recordings from the ground-based, runway center-line microphone of test points 1, 4, 6, 9, 11 and 14 are chosen to illustrate the important effects and findings observed in the measurements. The operating conditions of the test points are shown in table 4.

Table 4 Operating conditions for test points 1, 4, 6, 9, 11 and 14.

Parameters	Test Points					
	1	4	6	9	11	14
IAS (Target) [kts]	130	130	145	145	160	160
Gear setting	Up	Down	Up	Down	Up	Down
δ_f [deg]	0	0	0	0	0	0
n [RPM]	1600	1600	1600	1600	1600	1600

2. Generation of Noise Simulation Results

Simulation results are generated based on the recorded flight trajectories and aircraft performance of the aforementioned test points. Normally, the Hanson propeller model requires the torque and thrust loading along the propeller blade radius to calculate for propeller noise. However, at the time of writing, the authors do not possess the detailed 3D geometry of the F406 propeller, and therefore are not able to calculate a blade loading as a function of the blade radius. Instead a simplified approach is used, where the result is approximated by assuming a radius where all noise generation is concentrated, i.e. a point source, as detailed in [35].

The position of the point source along the radius of the propeller is calibrated based on the level time histories with high-fidelity simulations in a test case presented in [18]. The aircraft trajectories and performance data come from a previous measurement campaign of project L^2INK [15], in which measurements were conducted with a Dornier Do-228 (D-CODE). Since both the propellers mounted on D-ILAB and D-CODE comes from the MTV-27 family of MT Propeller [44] and are hence similar, it is possible to use the previous measurements as a basis for the selection of the point source location for this study.

Based on figure 6, a point source location at 65% of the blade radius is chosen for the initial immissions calculations. It should be noted that, however, existing models have shown underestimation of results of up to 10 dB as presented in [18], and this should be kept in mind for the upcoming simulation results. Research on which models are suitable is still ongoing, and the results of which will be presented for future work, and once improved propeller noise models has been developed, it will be used for future immissions assessments and subsequent investigations.

3. Comparison between Measurements & Simulation Results

The level time history of the A-weighted sound pressure level (L_A) is compared between the measurements and simulation results in figure 7 for the selected test points. Simulation results are generated using the flight performance data and trajectories measured. The ground attenuation of the noise immissions are taken into account by the calculations as detailed in the AzB (*Anleitung zur Berechnung von Lärmschutzbereichen*, or Instructions for the calculation of noise protection areas) [47], and then adding 3 dB to the results to account for the usage of ground microphones [48], whereas the atmospheric absorption during noise propagation is accounted for using the model detailed in the SAE ARP866A [27]. Airframe noise is calculated from the sum of the contributions from various sources. The contributions from the trailing-edge devices (i.e. flaps) and gear are shown in this case.

The level time histories from measurements and simulations are aligned by the $L_{A_{max}}$. From figure 7, a general increase in measurement and simulation levels can be seen from the deployment of the landing gear in figures 7b, 7d and 7f. This is mainly attributed to propeller and gear noise, since engine torque (T) and hence engine power are increased to overcome the additional drag caused by gear deployment. The interaction between the propeller wake and the gear also contributes to the increase in levels, since the main landing gear of the F406 is mounted aft of the propeller, and thus likely exposed to the propeller wake. The simulation results are underestimating levels compared to the measurements, which is in-line with previous results [15, 18]. There is a consistent underestimation for $L_{A_{max}}$ of 2 dBA as shown in

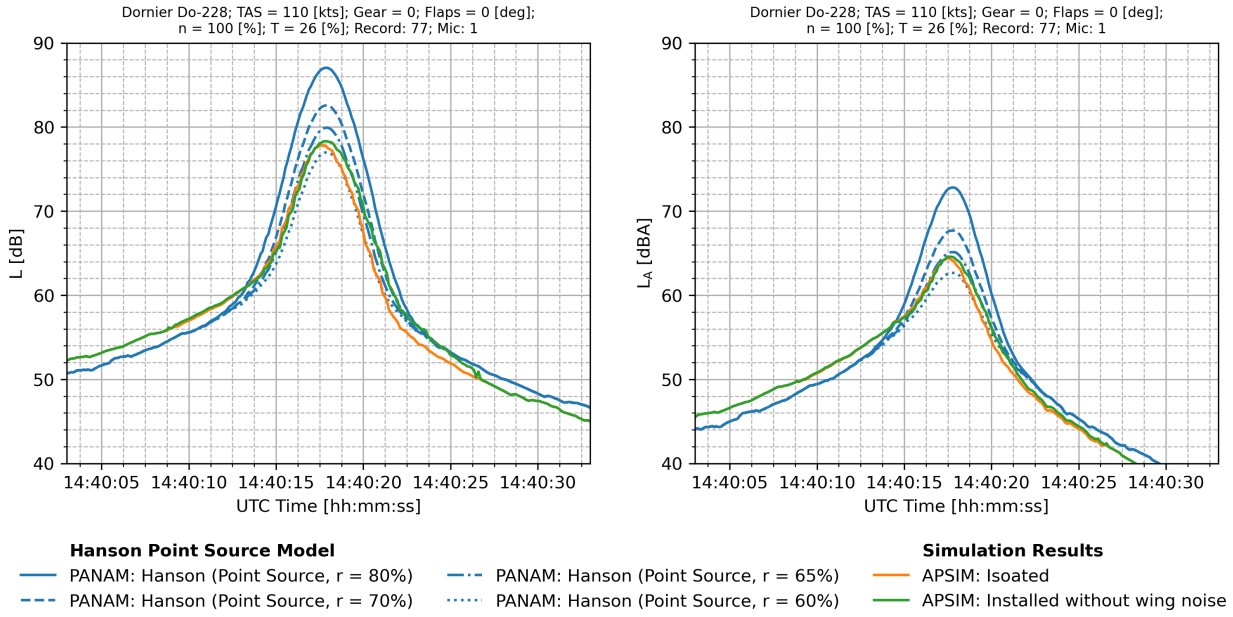

Fig. 6 Calibration of the point source location of the Hanson model based on L and L_A level time histories generated from high-fidelity simulation results for a test case presented in [18].

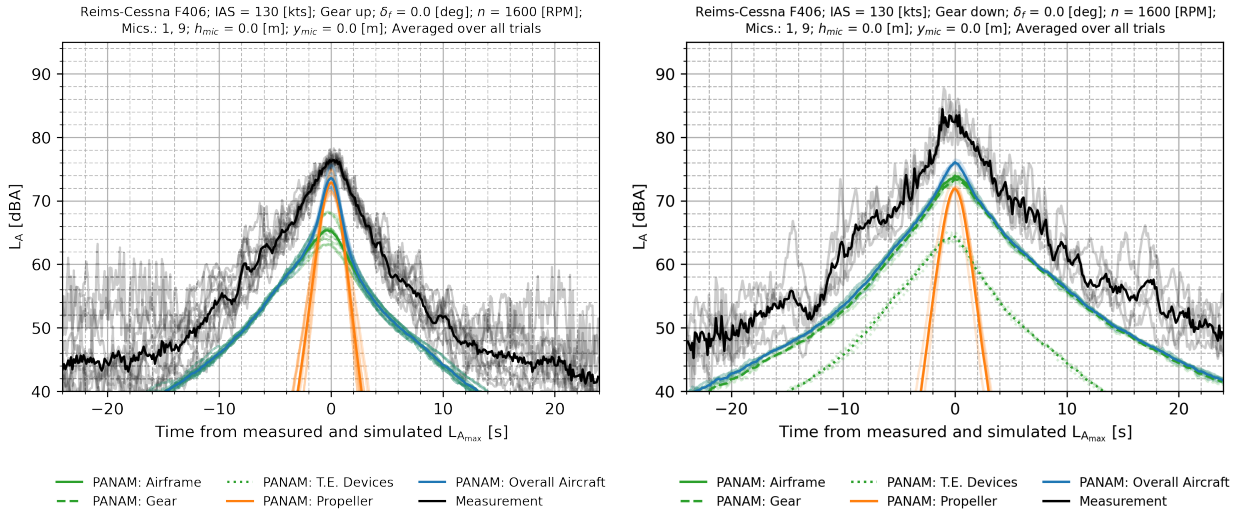

(a) Test Point 1 (IAS = 130 [kts], Gear Up). **(b) Test Point 4 (IAS = 130 [kts], Gear Down).**

Fig. 7 Level time histories comparisons at the runway center-line *.

* The translucent curves represent individual trials and simulations, while the opaque represent the average.

figures 7a, 7c and 7e for the aircraft in clean configuration, and not more than 7 dBA for the aircraft with the landing gear deployed in figures 7b, 7d and 7f. The underestimation in levels increases further away from $L_{A_{max}}$, where airframe noise becomes dominant. The underestimations could be attributed to the lack of consideration of propeller broadband noise and installation effects in PANAM currently, while the additional discrepancy in the cases where landing gear is deployed is hypothesized to be the interaction effects between the propeller wake and the landing gear. This hypothesis is also substantiated by the fact that, this effect was not previously observed for the Do-228 in [18], as the main landing gear is mounted far away from the propeller wake. The verification of this hypothesis is selected for future work.

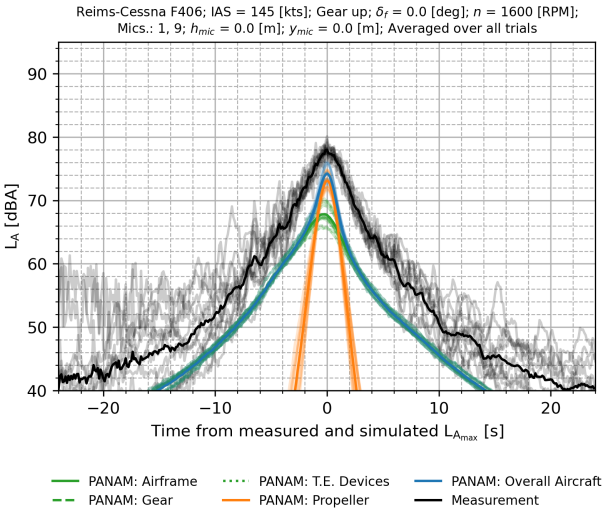

(c) Test Point 6 (IAS = 145 [kts], Gear Up).

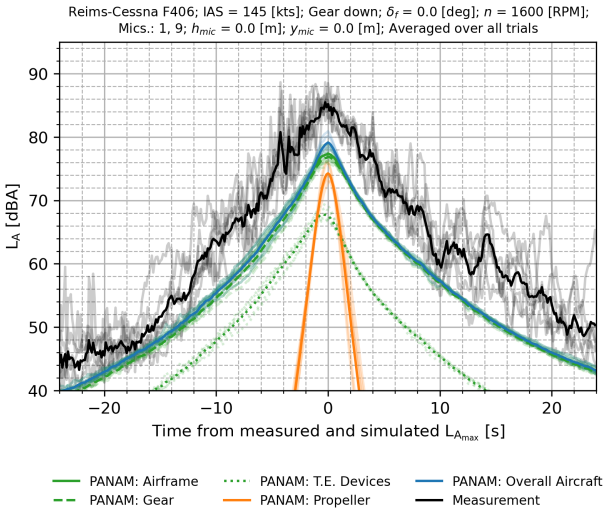

(d) Test Point 9 (IAS = 145 [kts], Gear Down).

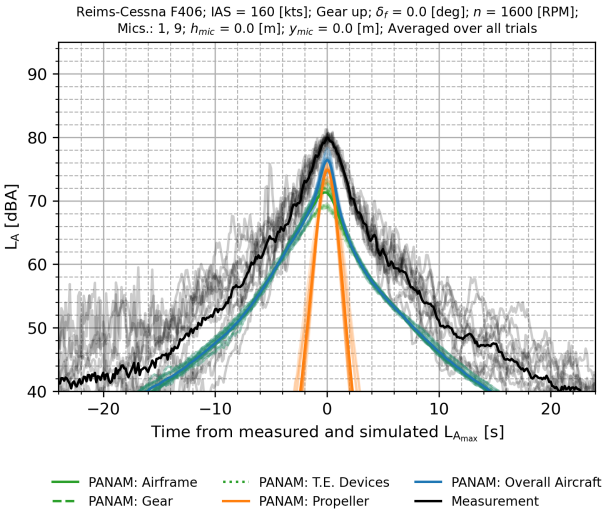

(e) Test Point 11 (IAS = 160 [kts], Gear Up).

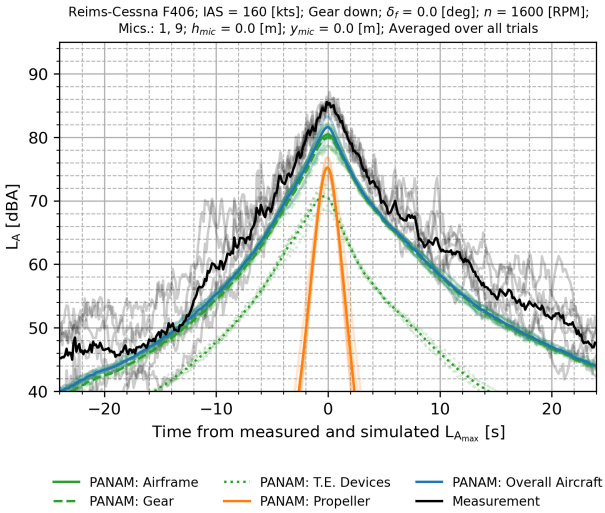

(f) Test Point 14 (IAS = 160 [kts], Gear Down).

Fig. 7 Level time histories comparisons at the runway center-line (cont.)*.

* The translucent curves represent individual trials and simulations, while the opaque represent the average.

With that being said, since the underestimation of $L_{A_{max}}$ levels are consistent throughout the trials at different aircraft configurations, the simulation process can be used to conduct immissions assessments for small propeller aircraft, as long as the possible underestimations of the results are taken into account.

V. Application of Simulation Process in Sensitivity Studies

The simulation process is applied to assess changes in the LTO operational parameters for the reference F406 aircraft to observe the sensitivity of the noise immissions to these parameters.

A. Reference Case

A reference immissions assessment for the F406 is first performed by generating trajectories for the F406 in approach and departure. The F406 POH [40] is consulted for the approach and departure procedures and the air speeds at different operational stages, such as climb, flap and gear deployment or retraction. Take-off power is assumed to the maximum power available, while climb power is assumed to be 90% of that of take-off power. FLIPNA results are as shown in figure 8. A generic, 4000 m long runway at mean sea level is assumed. The aircraft is performing a straight approach and departure at MLM and MTOM respectively.

Using the generated flight paths, the simulation process proceeds to the immissions assessment. A-weighted maximum sound pressure level ($L_{A_{max}}$) and the A-weighted sound exposure level (SEL) are chosen due to their ubiquity, relative straightforwardness in the calculation and relevance for certification [49].

The assessment is shown by $L_{A_{max}}$ contours in figure 10 and SEL contours in figure 11 for ground observers or microphones. The $L_{A_{max}}$ immission data is further examined over the ground track to see the noise source ranking over the flight path in figure 9. Ground attenuation and reflection effects are again considered in this case using the method previously detailed in section IV.C.3. From the contour plots in figures 10 and 11, it is possible to observe the effects of the deployment of different high-lift devices on the $L_{A_{max}}$ and SEL contours. The increase in $L_{A_{max}}$ and SEL levels as well as the contour widths from the deployment of the landing gear can be clearly seen at -10 km during approach, which is also confirmed by figure 8a, where it can be seen that the landing gear is deployed at that location, and figure 9a, where it can be confirmed that the increase in levels indeed results from an increased landing gear contribution. On the other hand, the extension of flaps does not seem to have as profound of an effect on the levels and shape of the $L_{A_{max}}$ and SEL contours compared to that of the landing gear, which is in line with existing PANAM result.

Using the illustration in figure 9b, it is also possible to easily assess whether the simulated aircraft complies to the noise level requirements per Annex 16, Volume I, Chapter 10 ("Propeller-driven aeroplanes not exceeding 8618 kg") to the Convention on International Civil Aviation [49] by ICAO. From chapter 10.4b, for the F406, a $L_{A_{max}}$ of 85 dBA measured from a ground mounted microphone is permitted at 2500 m from the point of break release.

In addition, for every aircraft certified to fly in Germany by the Federal Aviation Office (*Luftfahrt Bundesamt*), it is mandated that each aircraft must have a bespoke noise protection certificate (*Lärmschutzzeugnis*) that proves that the aircraft adheres to their corresponding noise certification levels. For D-ILAB, the aircraft recorded a $L_{A_{max}}$ of 74.6 dBA at the certification point as per chapter 10.4b, which is around 5 dB higher than that for the digital reference. However, the flight data at which this measurement is performed is not available, and therefore it is not possible to use this measurement as a validation point, merely as a point of reference.

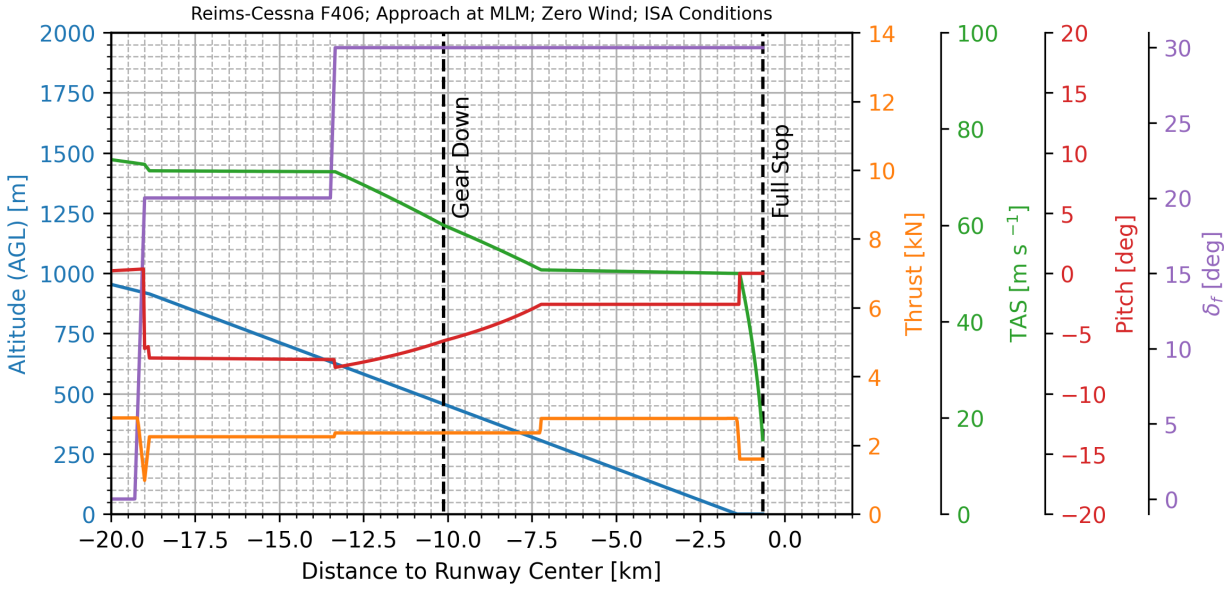

(a) Approach trajectory over distance.

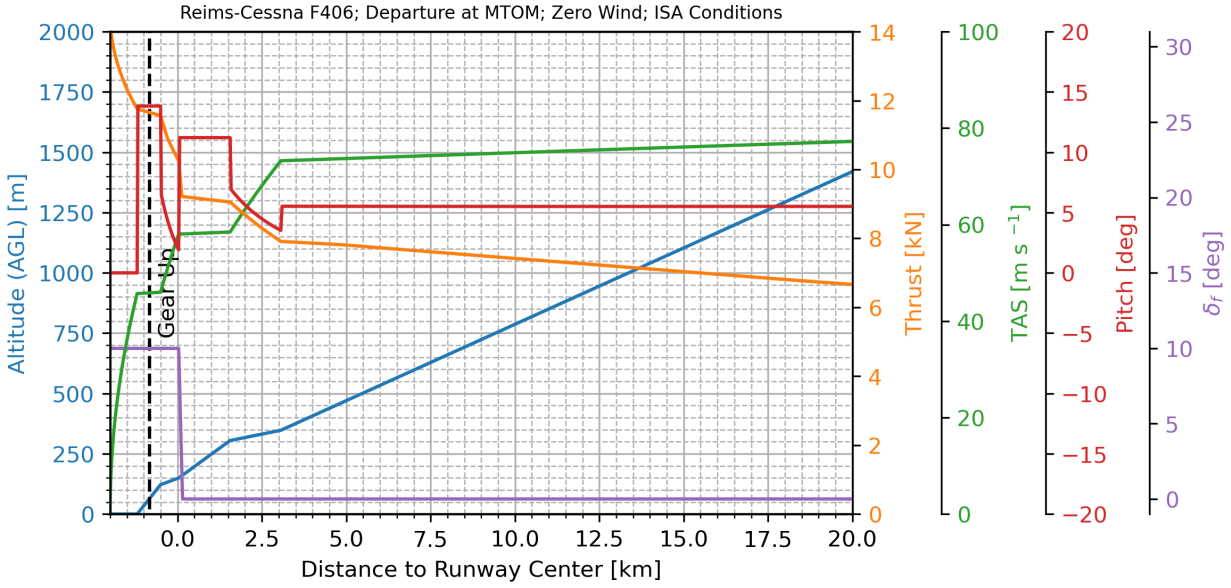

(b) Departure trajectory over distance.

Fig. 8 A general approach and departure case of the F406 calculated from FLIPNA*.

* The thrust dip during approach at -19 km is a software artefact which do not affect the noise immissions.

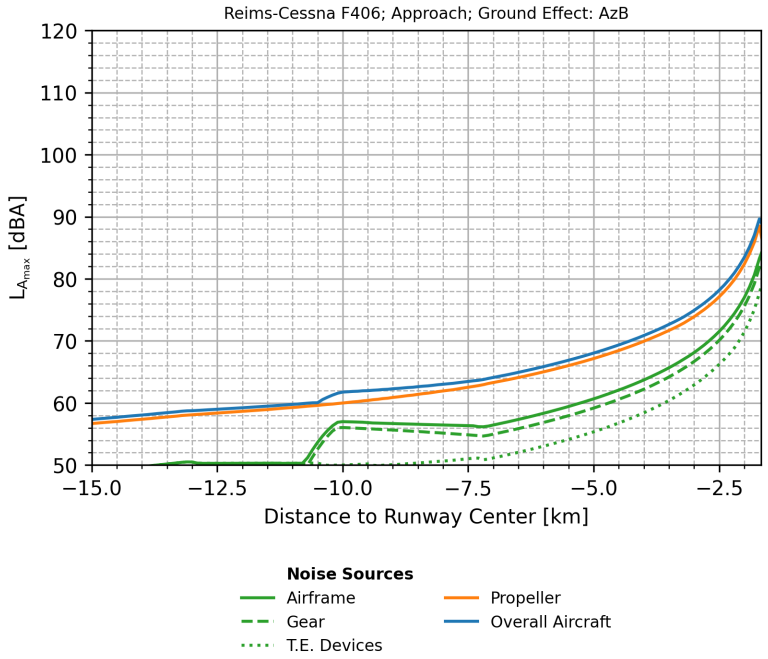

(a) Approach.

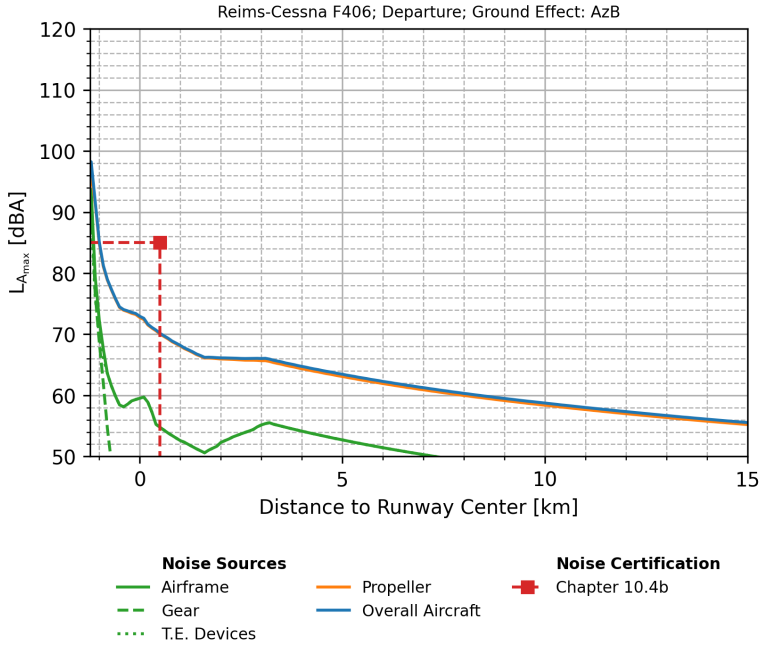

(b) Departure.

Fig. 9 Component $L_{A_{max}}$ predictions by PANAM over the ground track[*†].

[*] Airframe noise and its constituents are marked in green (Gear and trailing-edge devices are the most prominent airframe noise sources).

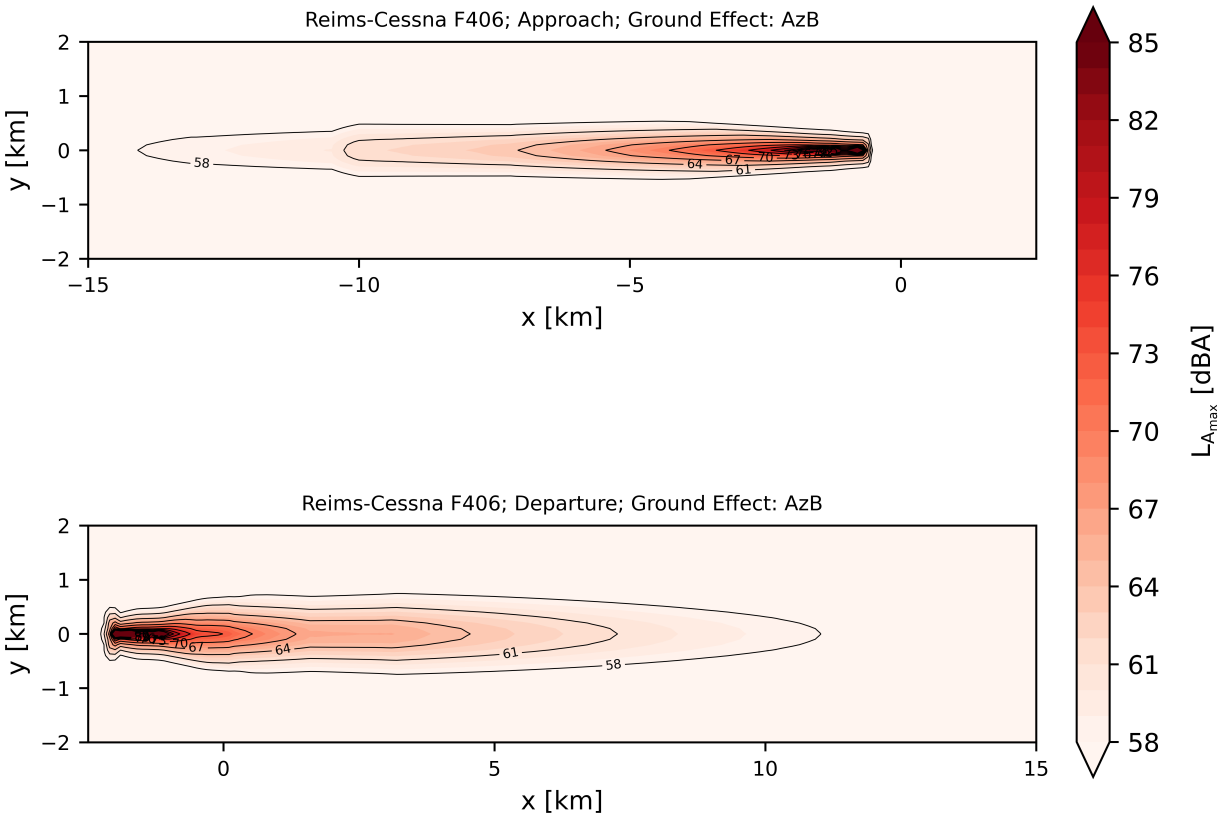

Fig. 10 $L_{A_{max}}$ contours predictions of the F406 in approach and departure.

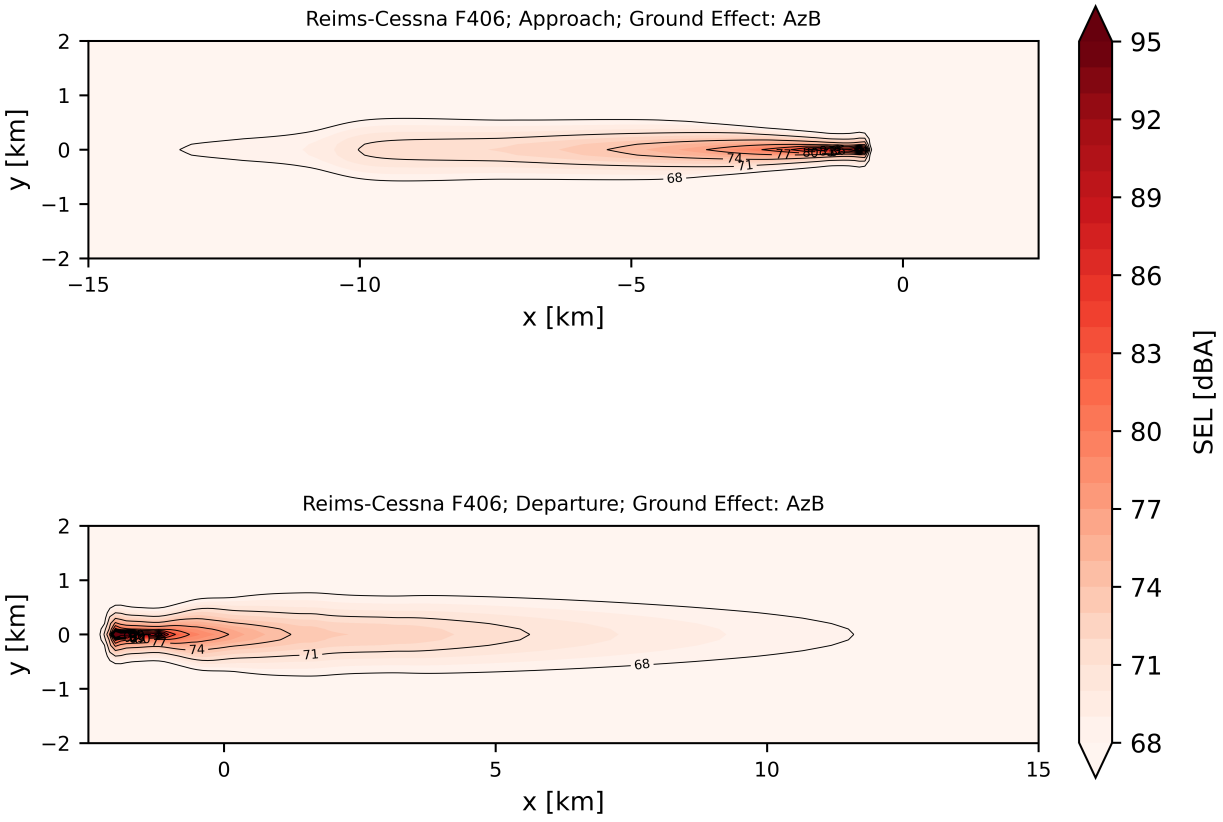

Fig. 11 SEL contours predictions of the F406 in approach and departure.

B. Noise Immissions Sensitivity Studies

Three studies are demonstrated by altering operational parameters in FLIPNA, namely the aircraft take-off mass, climb speed and climb power.

1. Study on Effect of Aircraft Payload

Provided that the climb power setting remains the same, a lighter aircraft would climb with a steeper climb angle, which would reduce the noise immissions below the flight path during departure as the aircraft will be higher from the ground at the equivalent longitudinal position after take-off. Take-off masses of 60% and 80% MTOM are tested. An additional test point a take-off weight of 4468 kg (approximately 105% MTOM) is also chosen to see if the reverse can be observed, as this is the MTOM of the increased gross weight variant of the F406 [42]. It is assumed that only minimal modifications to the F406 are needed to achieve the increased gross weight, and therefore the increase in MTOM can be modelled as a simple payload increase and would not necessitate a new conceptual aircraft design.

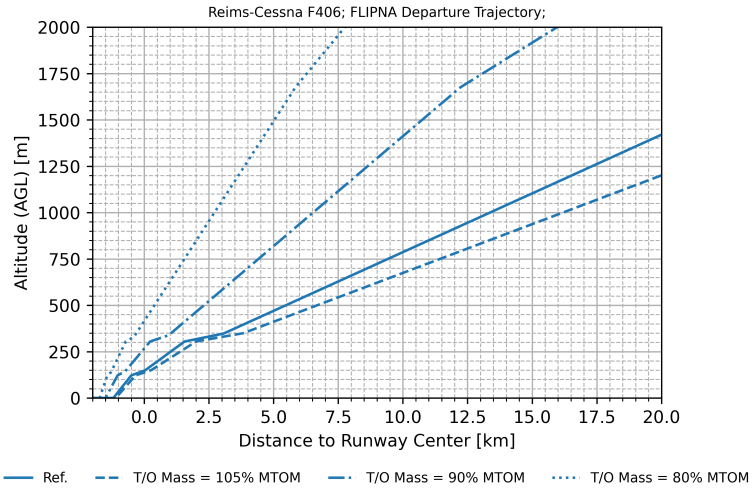

Fig. 12 Trajectory altitude over distance for different take-off masses.

Figure 12 and table 5 shows that the aircraft has a shorter take-off distance and has steeper flight path as the take-off mass decreases. The reverse if also observed with the case of the take-off mass at 105% MTOM. The effect of the new departure trajectory is seen as shifts in the $L_{A_{max}}$ curve over the ground track in figure 13a, where a lower take-off mass decreases the levels over the ground track while a higher take-off mass results in the reverse, an increase of just under 2 dBA for the case of 105% MTOM, and a up to 12 dBA for the case of 60% MTOM. This effect can also be observed from figures 14, 15, 16 and 17, where the overall area and length of the contours reduced. However, it should be noted that the sideline levels have increased as shown in figures 16 and 17, which is a result of the aircraft leaving the ground sooner and thus increasing the exposure that the aircraft creates in the early stages of the climb.

Table 5 Take-off distance at different take-off masses.

Take-off ground roll [m] at take-off mass of			
105% MTOM	**100% MTOM (Reference)**	**80% MTOM**	**60% MTOM**
921	803	520	292

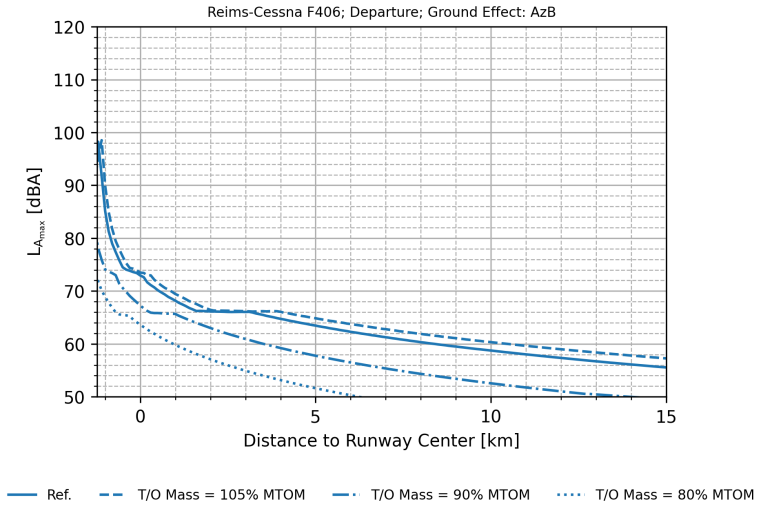

(a) $L_{A_{max}}$ over aircraft ground track.

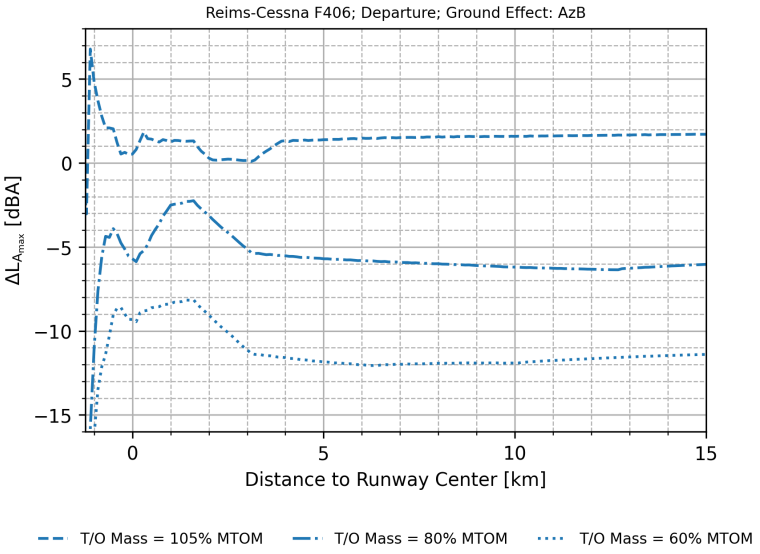

(b) $\Delta L_{A_{max}}$ over aircraft ground track.

Fig. 13 Effect of take-off masses on ground track noise immissions.

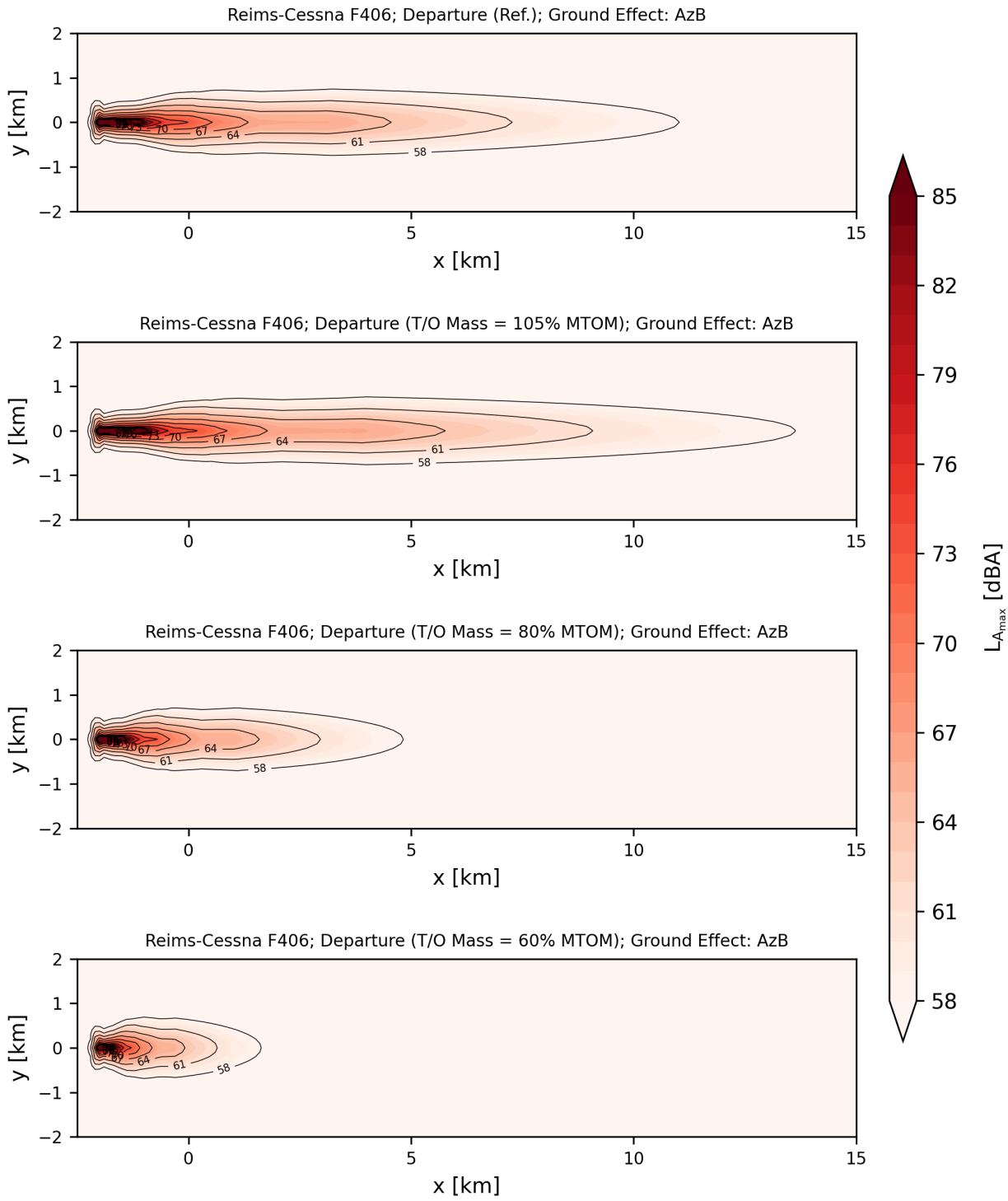

Fig. 14 $L_{A_{max}}$ contours at different take-off masses.

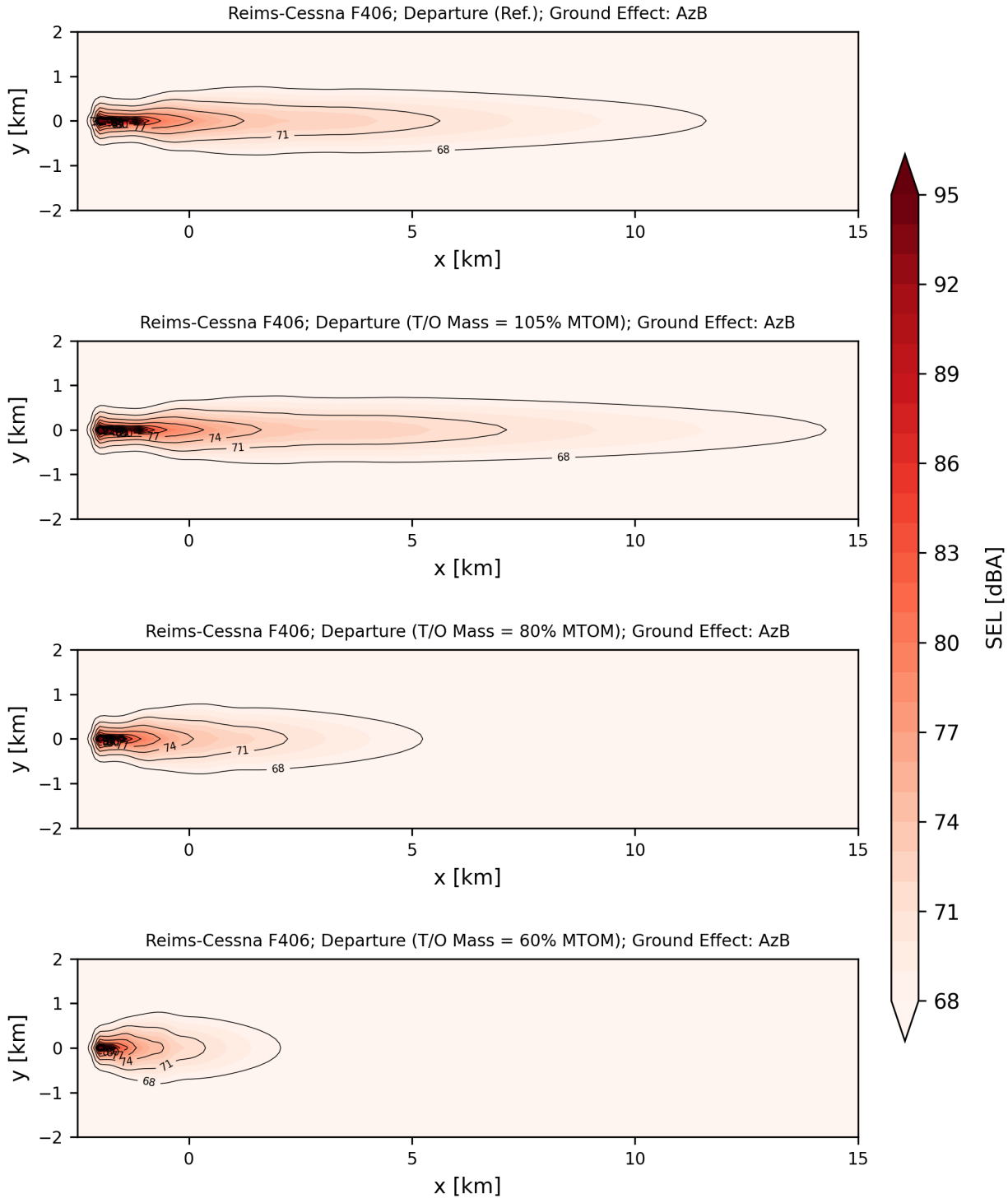

Fig. 15 SEL contours at different take-off masses.

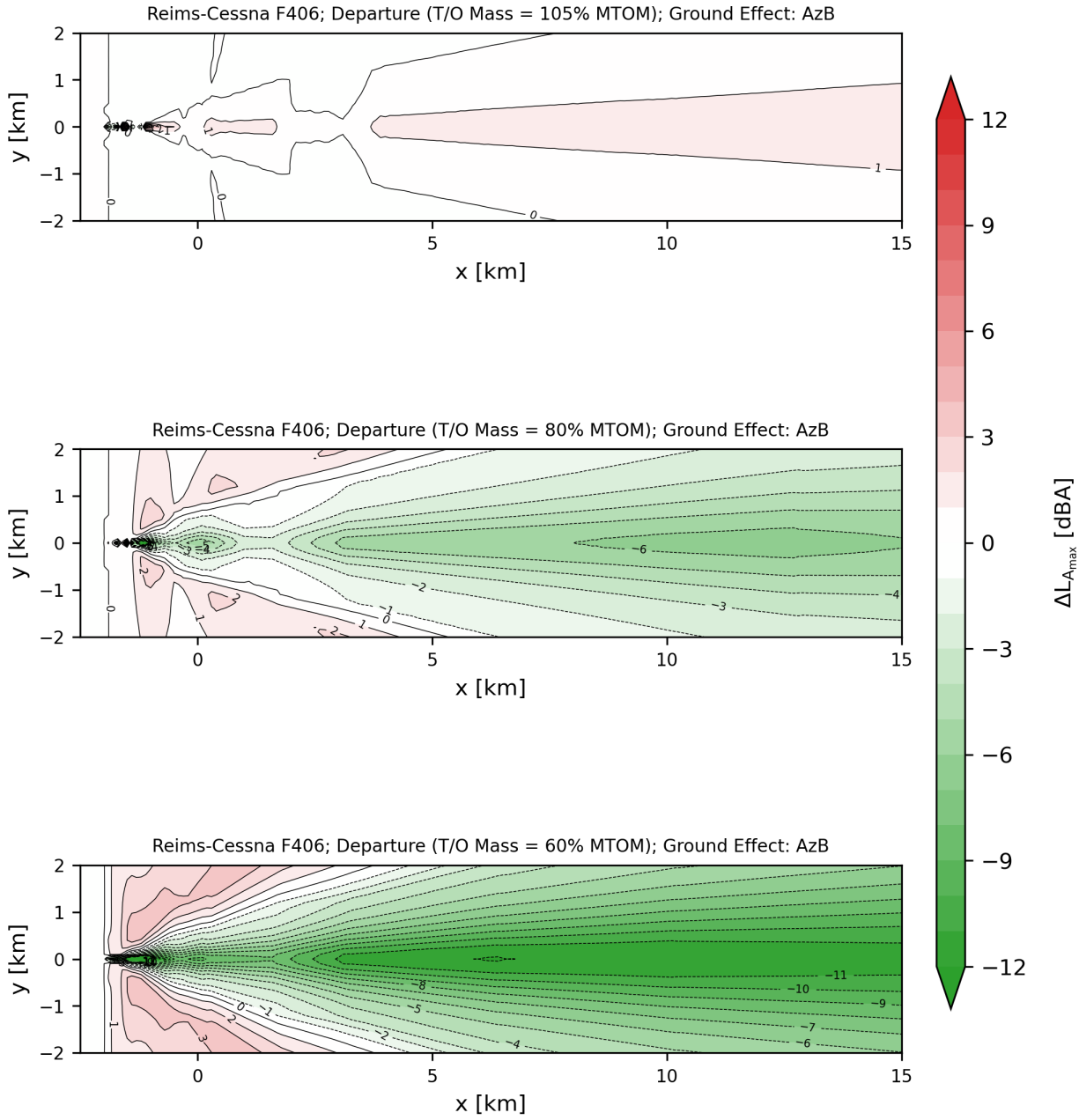

Fig. 16 $\Delta L_{A_{max}}$ contours at different take-off masses.

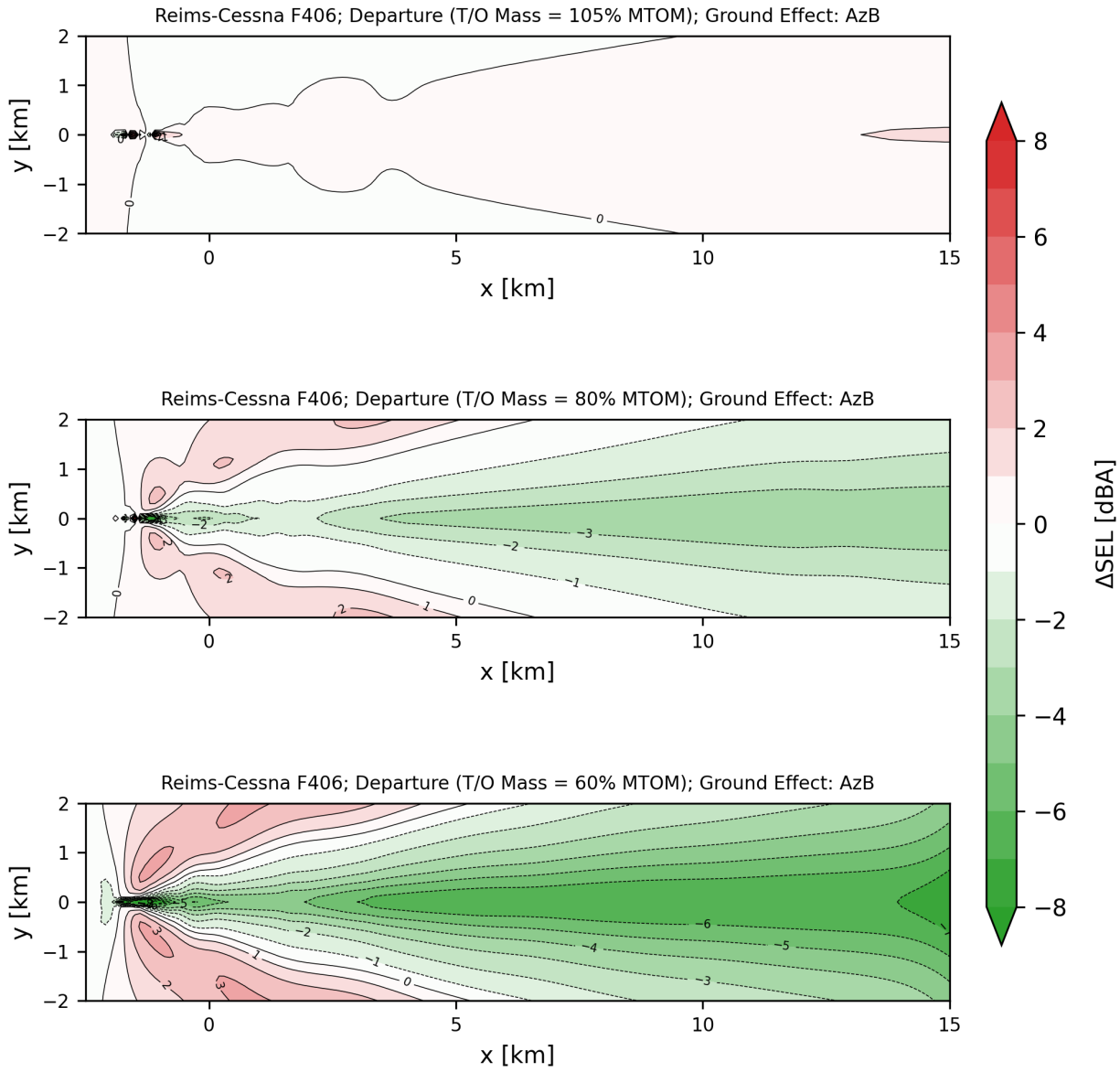

Fig. 17 ΔSEL contours at different take-off masses.

2. Study on Effect of Climb Speeds

In the reference departure shown in figure 8b, the F406 climbs at the recommended climb speed of 140 KIAS per the POH. Alternatively, climbing at V_y, the best rate-of-climb speed, would allow the aircraft to climb to the target altitude in the quickest time possible, while climbing at V_x, best angle-of-climb speed, would allow the aircraft to climb to the target altitude in the shortest ground track possible. Since noise immissions depends on the distance between the aircraft and the ground, climbing at V_x or V_y instead could reduce the noise immissions levels and exposure areas. For the F406, according the POH, V_y is 112 KIAS with no flaps and 109 KIAS with take-off flaps (δ_f = 10 [deg]), and V_x is 102 KIAS with take-off flaps [40].

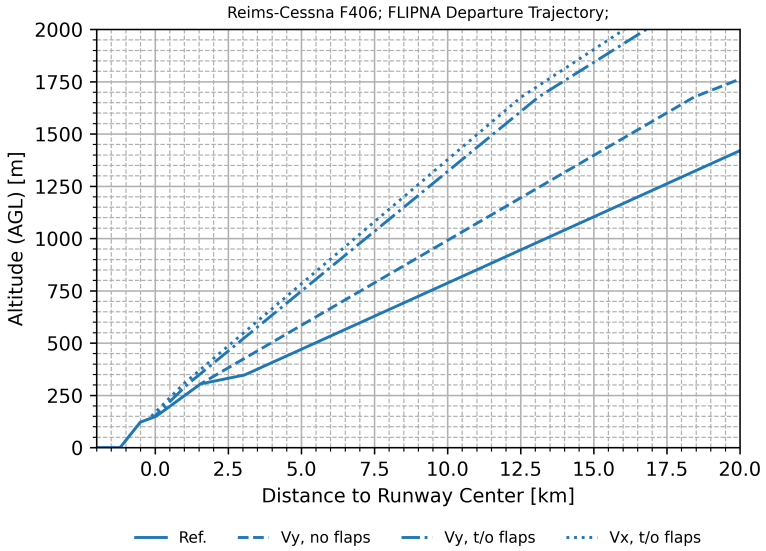

(a) Altitude over distance.

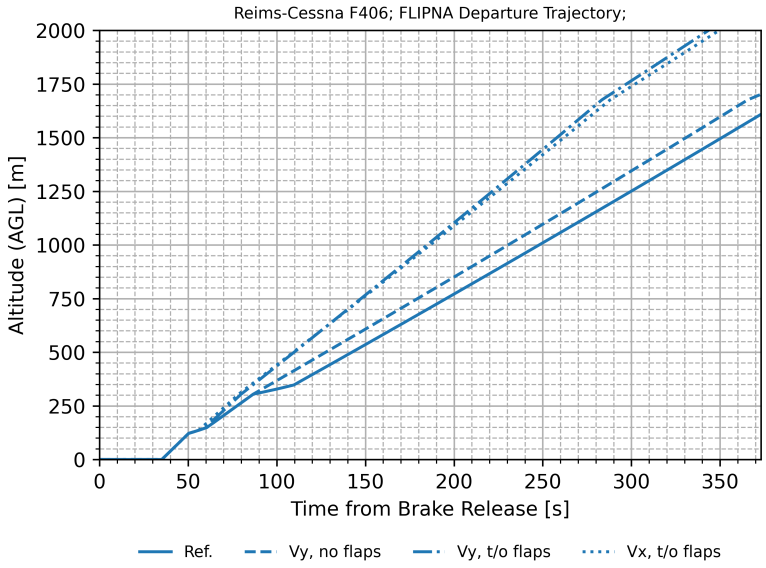

(b) Altitude over time.

Fig. 18 Trajectories from different climb speeds.

From figure 18, the effects of climbing at V_x and V_y and with/without flaps can be seen. The aircraft is able to climb with a higher angle and rate if V_y without flaps is maintained throughout the climb. This reduces the levels over the

ground track by about 3 dB as shown in figures 19a and 19b, and reduces the contour areas as in figures 20 and 21, although there are increases in the sideline levels as shown in figures 22 and 23. When the flaps kept in the take-off position throughout the climb, the levels over the ground track is further reduced by 2-4 dB, and the contour areas are further reduced as shown in the same figures.

The trajectories further differ when the aircraft climbs at V_x instead of V_y, as the altitude gain over distance of climbing at V_x out-performs that of V_y, while the opposite is true for altitude gain over time. This should in theory reduce the $L_{A_{max}}$ contour areas but increase the SEL contour areas for the V_x climb. However, the differences in resulting trajectories are not significant, resulting in a minimal changes in $L_{A_{max}}$ and SEL noise immissions over the ground track and contour areas.

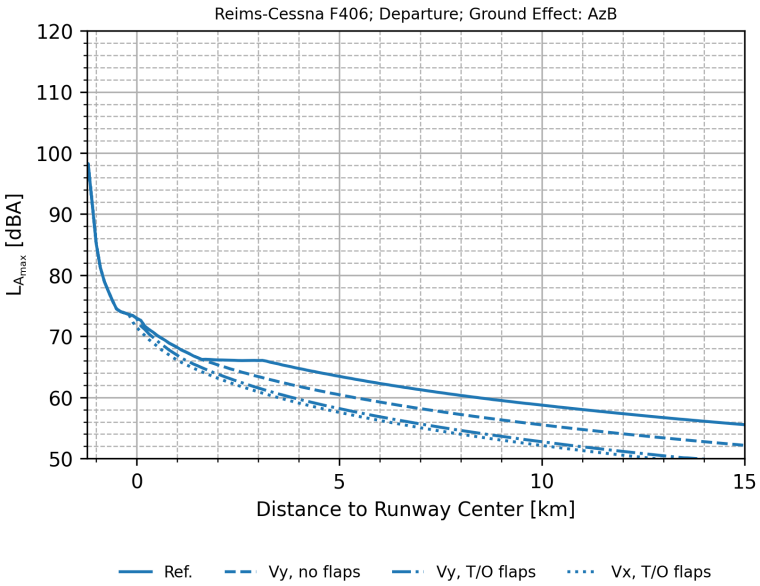

(a) $L_{A_{max}}$ over aircraft ground track.

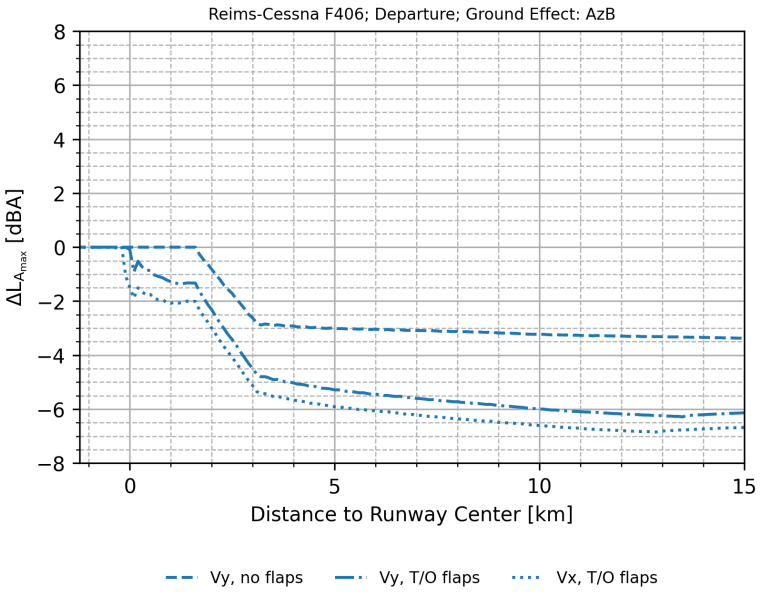

(b) $\Delta L_{A_{max}}$ over aircraft ground track.

Fig. 19 Effect of climb speed on ground track noise immissions.

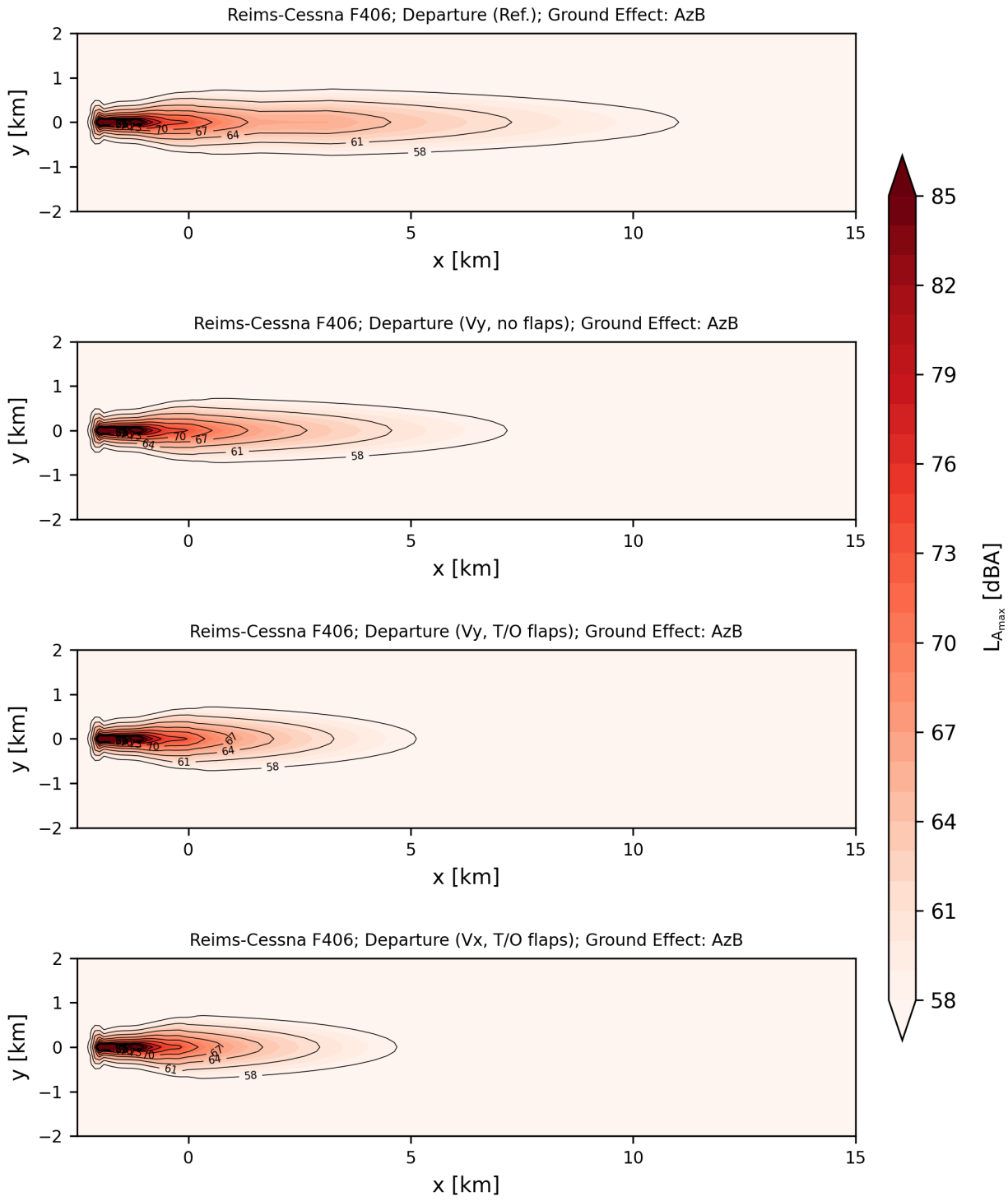

Fig. 20 $L_{A_{max}}$ contours at different climb speeds.

Additionally, from an operations perspective, performing a climb-out at V_x or V_y is not always practical as it is quite close to the minimum control airspeed with the flaps in take-off position at 90 KIAS for the F406 [40]. Any unforeseen weather conditions would put the aircraft at risk of stalling, and hence it is not recommended. Therefore to conclude, although altering the climb speed from V_y to V_x and hence climbing at a steeper angle reduces noise immissions, it adds additional risks to the operation of the aircraft during the climb-out phase.

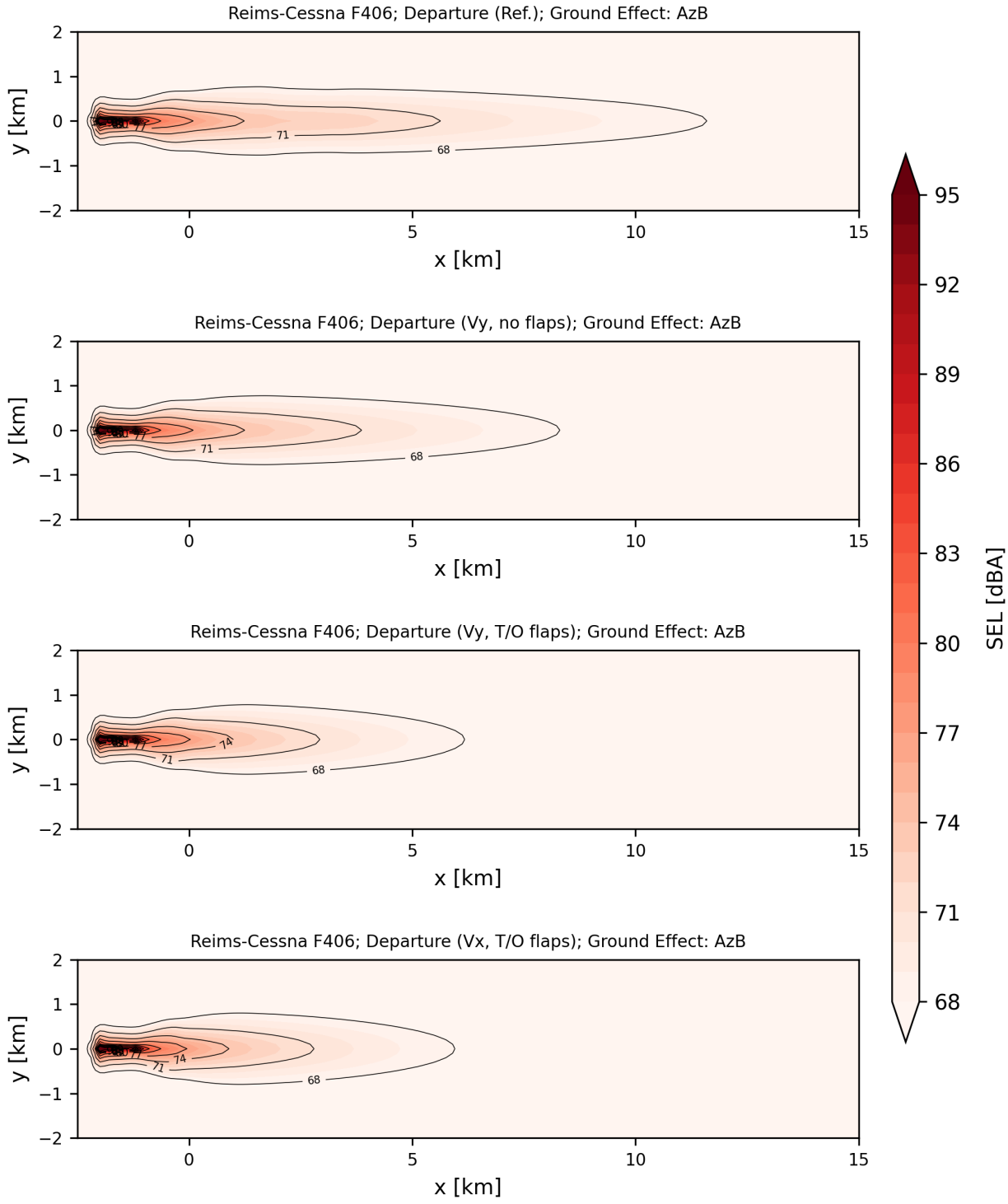

Fig. 21 SEL contours at different climb speeds.

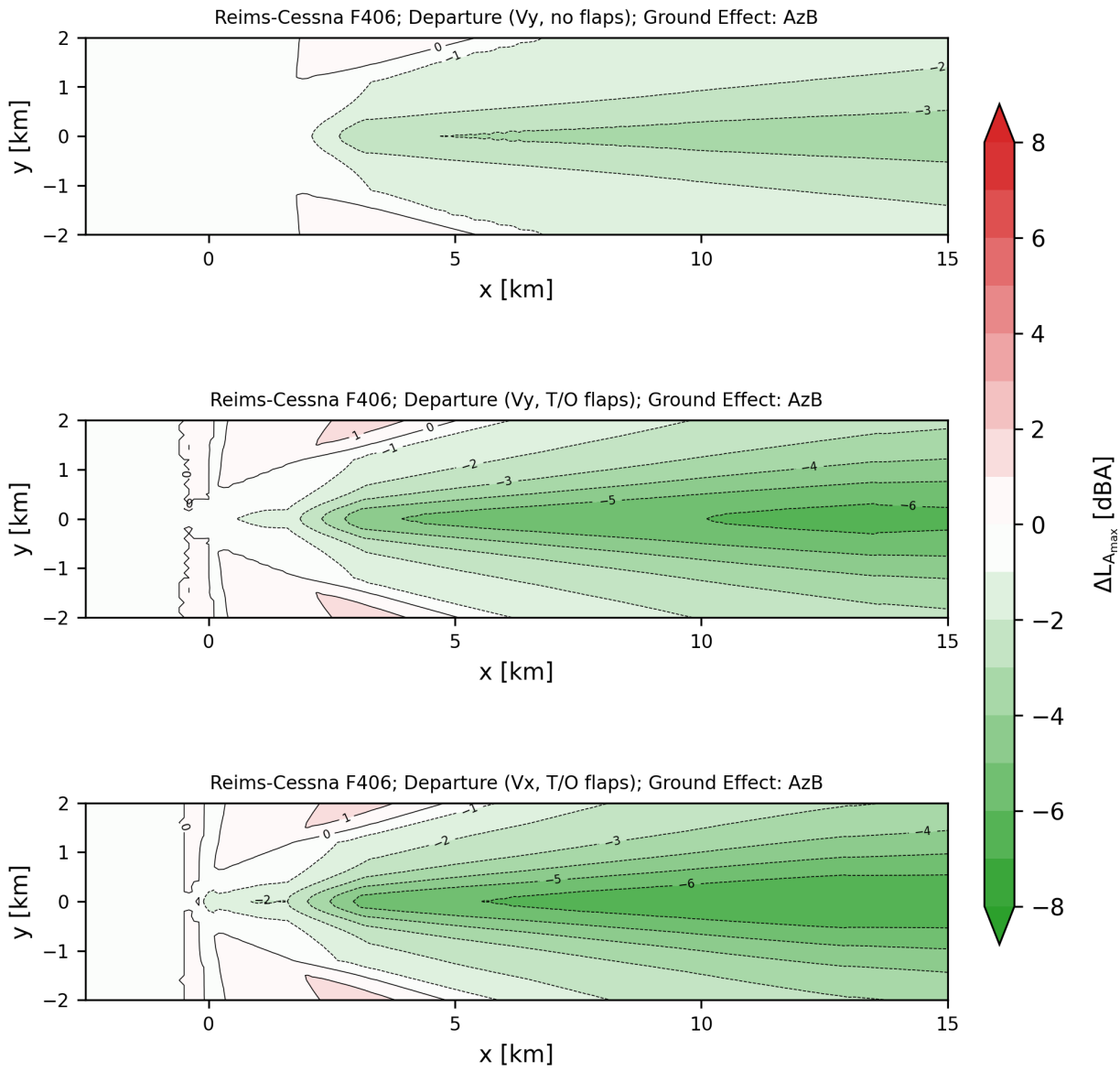

Fig. 22 $\Delta L_{A_{max}}$ contours at different climb speeds.

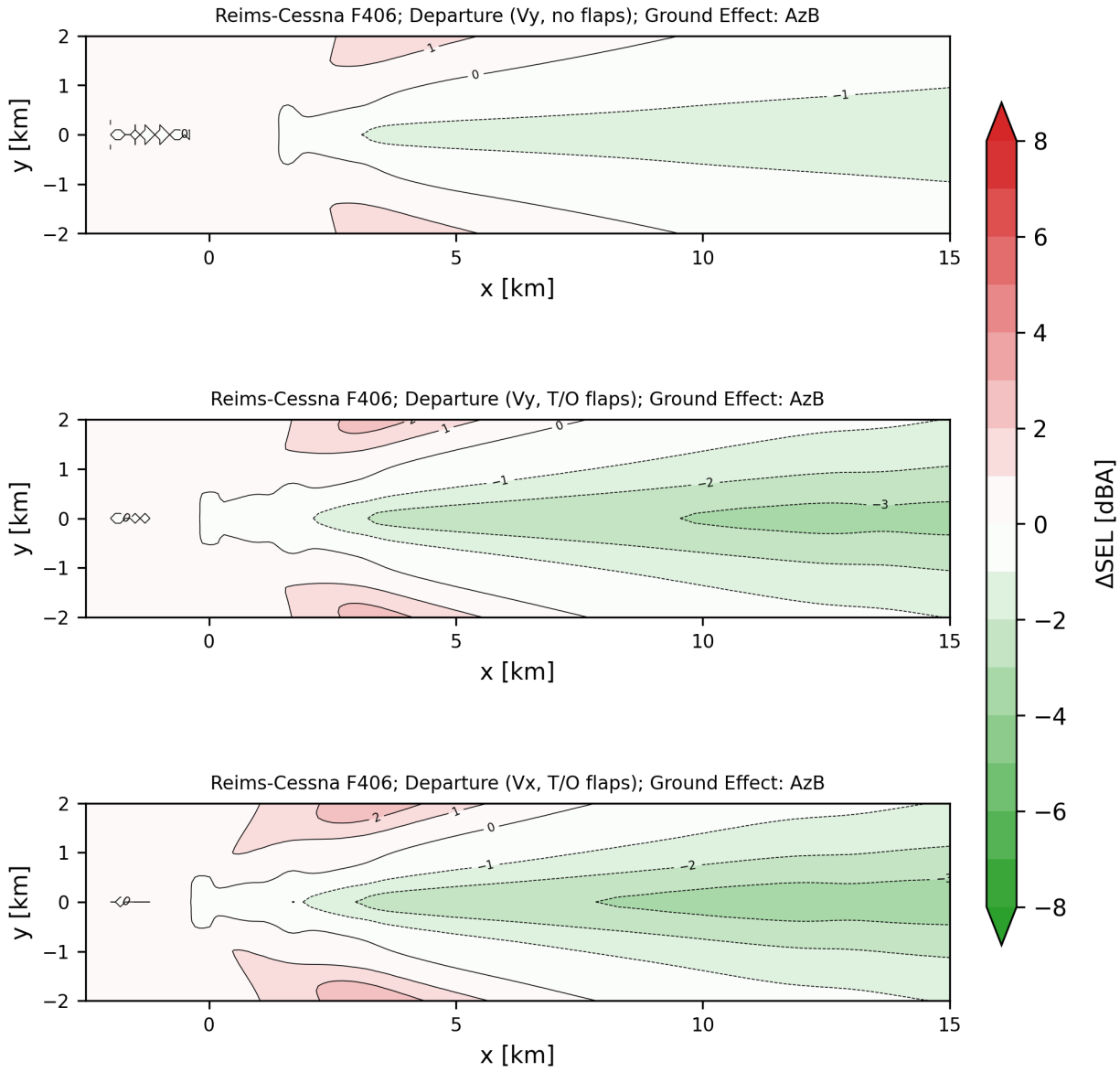

Fig. 23 ΔSEL contours at different climb speeds.

3. Study on Effect of Climb Power

As detailed in section IV.B, the climb power is set about 90% of that of the take-off power after the flaps have been retracted. Climbing at a higher power setting could help reduce the longitudinal spread of the noise immissions, i.e. the length of the $L_{A_{max}}$ and SEL contours, since the aircraft would climb at a more aggressive angle. However this might come at the expense of the lateral spread of the noise immissions, i.e. the width of the $L_{A_{max}}$ and SEL contours, since the engines are kept at a higher power setting at the initial climb phase.

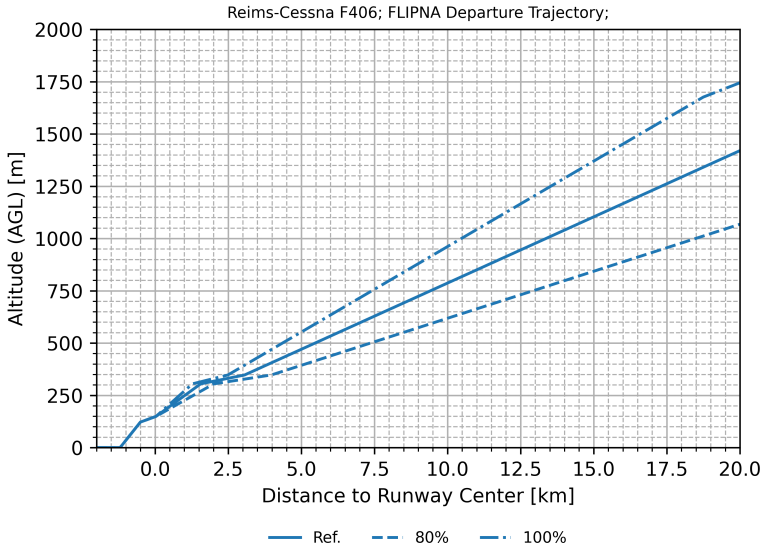

Fig. 24 Trajectory altitude over distance for different climb power settings.

As the climb power increases, the aircraft climbs at a steeper angle and reaches altitudes in a comparatively shorter ground track as seen in figure 24. The $L_{A_{max}}$ ground track levels shows differences of around 2 dB in figure 25a and 25b. The effect is not as large, as the effect of the shallower climb are mitigated by the lower power setting and hence less engine noise, and vice versa for the case of maximum climb power. The $L_{A_{max}}$ and SEL contours are shortened but increases in width as seen in figures 26 and 27. The effect on contour width can also be seen in figures 28 and 29, where the sideline levels increases with increasing climb power, with reasons similar to previous cases.

One downside of climbing with a higher power setting is that this would reduce the lifespan of the aircraft engine, should this measure be deployed over a considerable amount of time. This measure could hence be deployed for particularly noise sensitive areas where the aircraft has to perform a climb out on a non-regular basis.

Therefore to conclude, for the F406, climbing at a higher power setting can reduce the noise exposure area due to the higher climb rate. However, one should be aware of the increase in sideline levels and also the potential reduction in the lifespan of the aircraft engine.

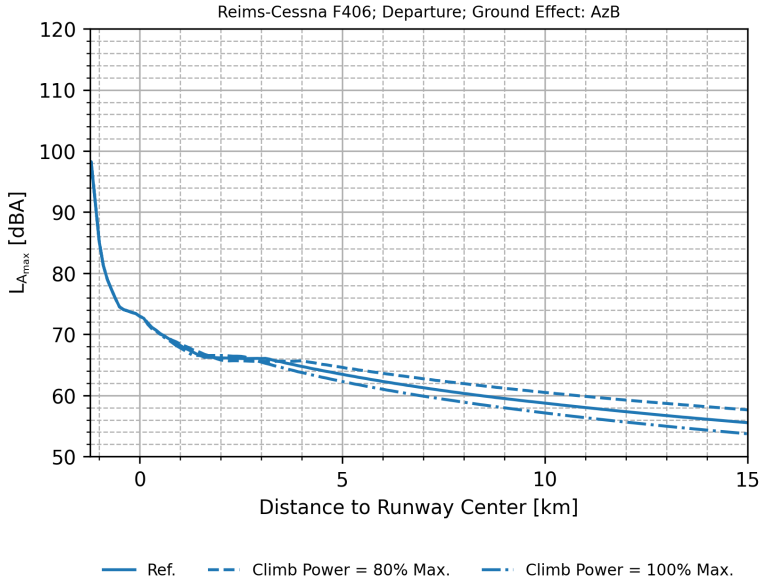

(a) $L_{A_{max}}$ over aircraft ground track.

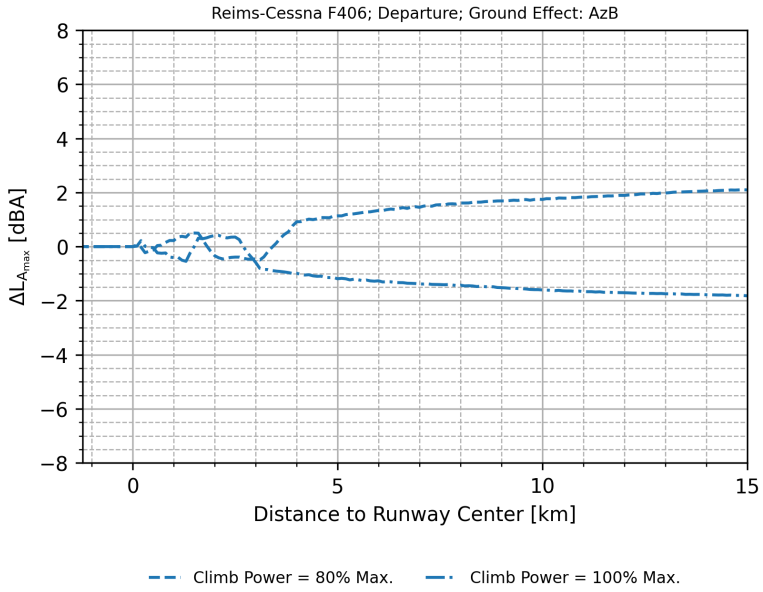

(b) $\Delta L_{A_{max}}$ over aircraft ground track.

Fig. 25 Effect of climb power setting on ground track noise immissions.

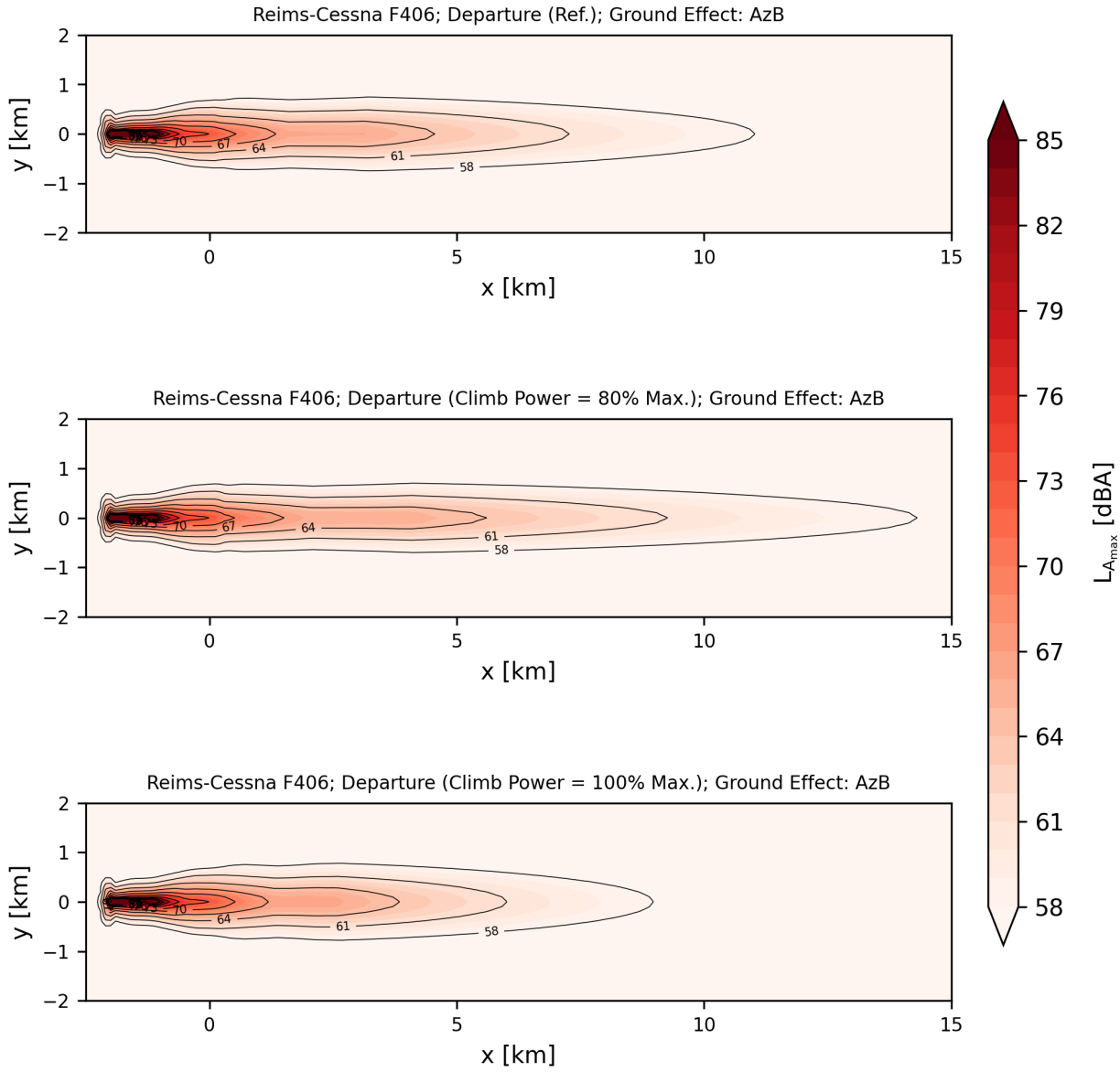

Fig. 26 $L_{A_{max}}$ contours at different climb power settings.

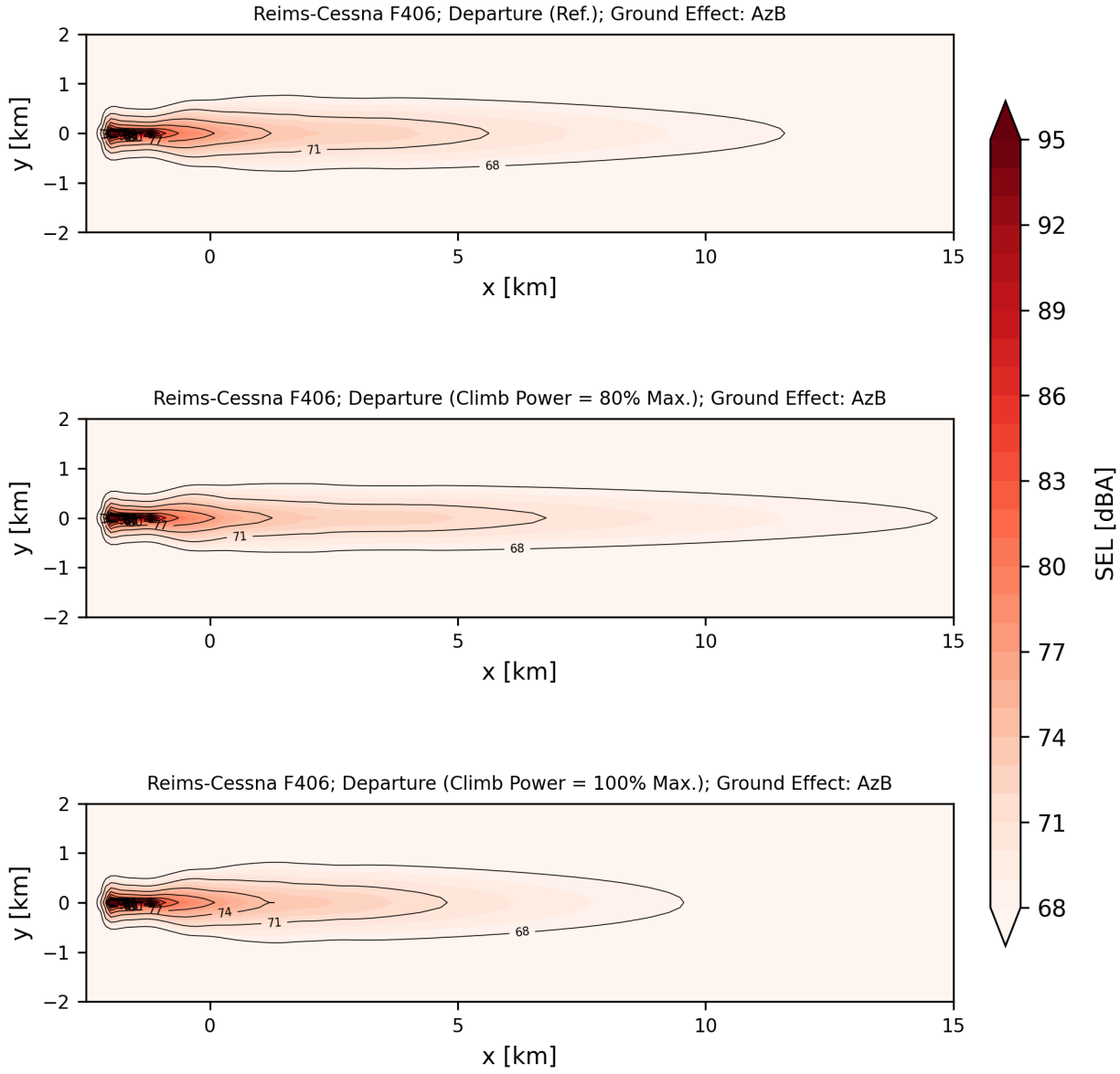

Fig. 27 SEL contours at different climb power settings.

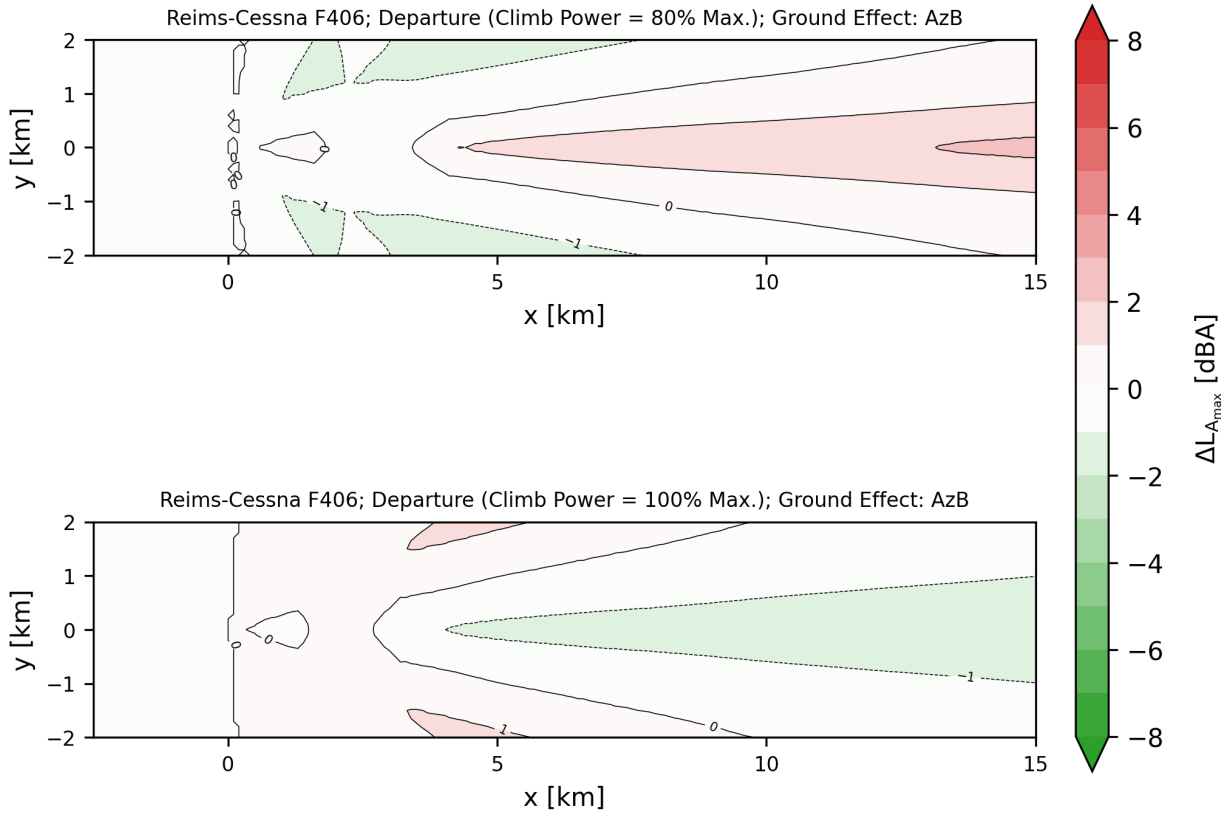

Fig. 28 $\Delta L_{A_{max}}$ contours at different climb power settings.

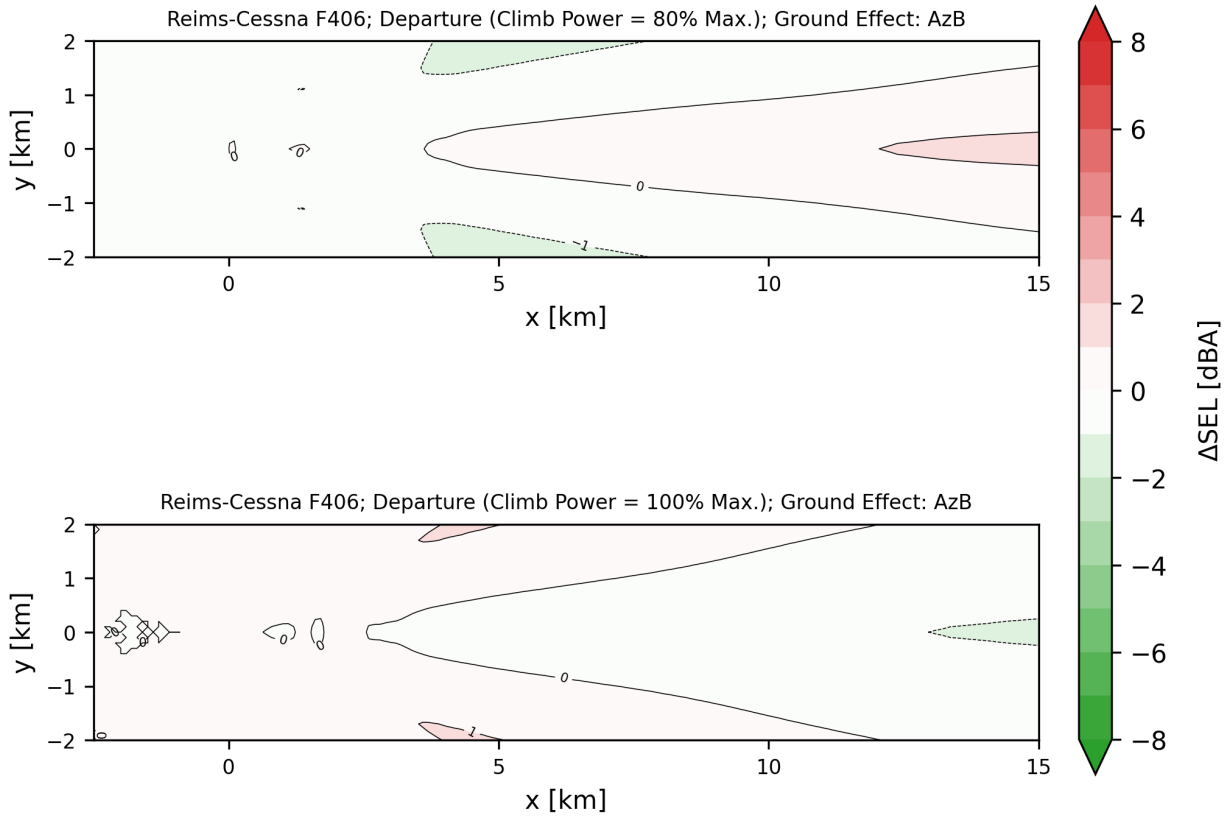

Fig. 29 ΔSEL contours at different climb power settings.

VI. Future Work

The identified limitations of the simulation process throughout this paper includes the underestimation of noise immissions by the simulation process compared to the measurements, with the underestimation increasing as the landing gear is deployed. These are attributed to propeller broadband noise, installation effects, and the interaction effects between the propeller wake and the main landing gear, which are currently not accounted for in PANAM. These limitations will be identified and addressed in future work. The results from the simulation process will be validated once the limitations have been addressed.

Future work will address the aforementioned limitations. It will also be focused on the expansion of the capabilities in aircraft, propeller and engine design, adapting noise propagation models which takes into account a turbulent atmosphere and other meteorological conditions [50], and including gaseous emissions dispersion simulations with LASPORT [51]. New mixed-fidelity propeller noise emission models that account for propeller installation effects, and methods to include interaction effects between the propeller wake, wing and landing gear will also be implemented.

The simulation process will then be further applied to evaluate low-noise small conceptual propeller aircraft. This could include retrofitting existing aircraft concepts by reducing the interaction between the propeller, wing and other high-lift devices or increasing the number of propeller blades to reduce the blade loading noise. Novel designs that employ a distributed propulsion architecture are also promising, as it generally reduces the blade loading, and also allows the aircraft to climb faster from the blown wing effect, which is advantageous for noise mitigation. Bespoke noise mitigation procedures for the low-noise conceptual aircraft will also be developed.

VII. Conclusion

This paper presents the progress on the development of a simulation process that assesses the noise immissions of CS-23 propeller aircraft concepts. Current work focuses on the realization of the simulation process itself, which entails the conceptual design of the reference aircraft, the Reims-Cessna F406 Caravan II, the generation of flight paths for a general approach and departure case for the F406, and the calculation of $L_{A_{max}}$ and SEL ground immissions using the Hanson propeller noise model after comparing it with results from other models in previous work.

The results from the simulation process are also compared to that obtained from a measurement campaign where a F406 performed constant speed flyovers over a set of microphones. From which, the A-weighted sound pressure level (L_A) time histories are extracted, and shows that the simulation results currently underestimate the ground noise immissions by about 2 dBA at $L_{A_{max}}$ for the aircraft in a clean configuration, with the underestimation increasing to up to 7 dBA when the landing gear is deployed. This is in line with previous results, and hence future work will focus on addressing propeller installation effects, the deficiencies in modelling of the interaction noise between the propeller wake and high-lift devices such as flaps and the landing gear, as well as propeller broadband noise. Investigations into the suitability and validation of various propeller noise models are also ongoing.

The simulation process is applied to assess propeller aircraft noise immissions in three sensitivity studies of the F406 in departure, by modifying the take-off weight, climb speed and climb power and showing how the modification of these parameters affect the $L_{A_{max}}$ and SEL ground noise immissions. Results show that measures which result in the aircraft leaving the ground in a shorter ground track and time are beneficial for the noise immissions over the ground track, albeit at the expense of small increases in the sideline levels. Operational factors must also be considered to determine whether these noise mitigation measures are feasible. Future work will be focused addressing the identified limitations, and the expansion of its capabilities in simulating the effects of a turbulent atmosphere and meteorological conditions on noise propagation, propeller installation effects, interaction effects between the propeller wake and airframe components, and finally, the assessment of novel, low-noise small conceptual propeller aircraft.

Acknowledgments

This work is part of project L^2INK led by the DLR Institute of Aerodynamics and Flow Technology, funded by the German Federal Ministry of Economic Affairs and Climate Action (*Bundesministerium für Wirtschaft und Energie*). The authors would also like to acknowledge the DLR Institute of System Architectures in Aeronautics for the provision of and assistance in software.

References

[1] *Strategic Research and Innovation Agenda*. 2021. URL: https://clean-aviation.eu/sites/default/files/2022-01/CAJU-GB-2021-12-16-SRIA_en.pdf.

[2] Rolf Henke, Tim Lammering, and Eckhard Anton. "Impact of an Innovative Quiet Regional Aircraft on the Air Transportation System". In: *Journal of Aircraft* 47.3 (2010), pp. 875–886. DOI: https://doi.org/10.2514/1.45785.

[3] Silent Aircraft Initiative. URL: http://silentaircraft.org/.

[4] Lothar Bertsch et al. "10 years of joint research at DLR and TU Braunschweig toward low-noise aircraft design - what did we achieve?" In: *Aeronautics and Aerospace Open Access Journal* 3.2 (2019), pp. 89–104. DOI: https://doi.org/10.15406/aaoaj.2019.03.00085.

[5] Lothar Bertsch. *Noise Prediction within Conceptual Aircraft Design*. Tech. rep. Technische Universität Braunschweig, Aug. 2013. URL: https://elib.dlr.de/84386/.

[6] Jason Blinstrub. *Immission-Based Noise Reduction within Conceptual Aircraft Design*. Tech. rep. 2019. URL: https://elib.dlr.de/127483/.

[7] Felix Wienke et al. "System Noise Assessment of Conceptual Tube-and-Wing and Blended-Wing-Body Aircraft Designs". In: *AIAA Aviation 2023 Forum*. Ed. by AIAA. AIAA, June 2023. URL: https://elib.dlr.de/196513/.

[8] Milo D. Dahl. *Assessment of NASA's Aircraft Noise Prediction Capability*. Tech. rep. NASA/TP—2012-215653. July 2012. URL: https://ntrs.nasa.gov/api/citations/20120012957/downloads/20120012957.pdf.

[9] Leonard Lopes and Casey Burley. "Design of the Next Generation Aircraft Noise Prediction Program: ANOPP2". In: *17th AIAA/CEAS Aeroacoustics Conference (32nd AIAA Aeroacoustics Conference)*. DOI: 10.2514/6.2011-2854. eprint: https://arc.aiaa.org/doi/pdf/10.2514/6.2011-2854. URL: https://arc.aiaa.org/doi/abs/10.2514/6.2011-2854.

[10] Patrice Malbéqui, Yannick Rozenberg, and Jean Bulté. "Aircraft Noise Prediction in the IESTA Program". In: *InterNoise Conference*. Sept. 2011. URL: https://api.semanticscholar.org/CorpusID:164213435.

[11] Junichi Akatsuka. *Development of Aircraft Noise Estimation Tool (AiNEST)*. Tech. rep. (In Japanese). Japan Aerospace Exploration Agency, Feb. 2017. URL: https://jaxa.repo.nii.ac.jp/records/1874.

[12] Bieke von den Hoff, Dick Simons, and Mirjam Snellen. "Breakdown of Propeller Aircraft Noise by applying Conventional Beamforming jointly with Imaging using the Rotating Source Identifier". In: June 2022.

[13] Stanislaus Reitenbach et al. "Collaborative Aircraft Engine Preliminary Design using a Virtual Engine Platform, Part A: Architecture and Methodology". In: *AIAA SciTech Forum 2020*. Ed. by AIAA SciTech Forum 2020. Jan. 2020. URL: https://elib.dlr.de/134141/.

[14] D. Heimann, A. Schady, and J. Feng. "Atmospheric acoustics". In: ed. by U. Schumann. Research Topics in Aerospace. Springer-Verlag Berlin Heidelberg, 2012, pp. 203–218. URL: https://elib.dlr.de/77774/.

[15] Antje Feldhusen-Hoffmann et al. "Noise and local pollutants of small aircraft: overview of simulation activities and of the first flight test within the DLR project L2INK". In: *AIAA Aviation 2023 Forum*. Ed. by AIAA. AIAA, June 2023, pp. 1–20. URL: https://elib.dlr.de/196509/.

[16] Brigitte Boden et al. "RCE: An Integration Environment for Engineering and Science". In: *SoftwareX* 15 (July 2021). Preprint verfügbar unter https://arxiv.org/abs/1908.03461. URL: https://elib.dlr.de/131958/.

[17] M. Alder et al. "Recent Advances in Establishing a Common Language for Aircraft Design with CPACS". In: *Aerospace Europe Conference*. 2020. URL: https://elib.dlr.de/134341/.

[18] Jatin Manghnani et al. "A First Principle Based Approach for Prediction of Tonal Noise From Isolated and Installed Propeller". In: *30th AIAA/CEAS Aeroacoustics Conference (2024)*. DOI: 10.2514/6.2024-3382. eprint: https://arc.aiaa.org/doi/pdf/10.2514/6.2024-3382. URL: https://arc.aiaa.org/doi/abs/10.2514/6.2024-3382.

[19] Sirine Gharbi, Arthur Schady, and Katharina Maria Elsen. "Investigation of the Impact of Real Atmospheric Conditions on Noise Propagation from Small Aircraft Technologies". In: *10th Convention of the European Acoustics Association*. 10th Convention of the European Acoustics Association, Sept. 2023. URL: https://elib.dlr.de/203402/.

[20] S. Woehler et al. "Preliminary Aircraft Design within a Multidisciplinary and Multifidelity Design Environment". In: *Aerospace Europe Conference*. 2020. URL: https://elib.dlr.de/185515/.

[21] *Report on Standard Method of Computing Noise Contours around Civil Airports*. Tech. rep. ECAC.CEAC Doc 29. 4th Edition. European Civil Aviation Conference, Dec. 2016. URL: https://www.ecac-ceac.org/documents/ecac-documents-and-international-agreements.

[22] M. Pott-Pollenske et al. "Validation of a Semiempirical Airframe Noise Prediction Method through Dedicated A319 Flyover Noise Measurements". In: *8th AIAA/CEAS Aeroacoustics Conference; Breckenridge (usa), 17.-19.06.2002*. LIDO-Berichtsjahr=2003, monograph_id=AIAA 2002-2470, 2002. URL: https://elib.dlr.de/12574/.

[23] W. Dobrzynski et al. "A European Study on Landing Gear Airframe Noise Sources". In: *6th AIAA/CEAS Aeroacoustics Conference, Lahaina/Hawaii (usa), 12.-14.06.2000*. LIDO-Berichtsjahr=2001, monograph_id=AIAA 2000-1971, 2000. URL: https://elib.dlr.de/13307/.

[24] Werner Dobrzynski and Michael Pott-Pollenske. "Slat Noise Source Studies for Farfield Noise Prediction". In: *CD-Proceedings*. LIDO-Berichtsjahr=2002, 2001. URL: https://elib.dlr.de/12436/.

[25] Karl Rossignol. "Development of an empirical prediction model for flap side-edge noise". In: *16th AIAA/CEAS Aeroacoustics Conference*. June 2010. URL: https://elib.dlr.de/68187/.

[26] Karl Rossignol. "Empirical prediction of flap tip noise". In: *17th AIAA/CEAS Aeroacoustics Conference (32nd AIAA Aeroacoustics Conference)*. DOI: 10.2514/6.2011-2733. eprint: https://arc.aiaa.org/doi/pdf/10.2514/6.2011-2733. URL: https://arc.aiaa.org/doi/abs/10.2514/6.2011-2733.

[27] A-21 Aircraft Noise Measurement Aviation Emission Modeling. *STANDARD VALUES OF ATMOSPHERIC ABSORPTION AS A FUNCTION OF TEMPERATURE AND HUMIDITY*. Mar. 1975. DOI: https://doi.org/10.4271/ARP866A. URL: https://doi.org/10.4271/ARP866A.

[28] International Organization for Standardization (ISO). *Acoustics—Attenuation of Sound during Propagation Outdoors. Part 1: Calculation of the Absorption of Sound by the Atmosphere*. Tech. rep. ISO 9613-1:1993. 1993.

[29] C.F. Chien and W.W. Soroka. "Sound propagation along an impedance plane". In: *Journal of Sound and Vibration* 43.1 (1975), pp. 9–20. ISSN: 0022-460X. DOI: https://doi.org/10.1016/0022-460X(75)90200-X. URL: https://www.sciencedirect.com/science/article/pii/0022460X7590200X.

[30] Lothar Bertsch et al. "System noise assessment of a tube-and-wing aircraft with geared turbofan engines". In: *Journal of Aircraft*. Journal of Aircraft 56.4 (Apr. 2019). Ed. by AIAA, pp. 1577–1596. URL: https://elib.dlr.de/118513/.

[31] Donald B. Hanson. "Helicoidal Surface Theory for Harmonic Noise of Propellers in the Far Field". In: *AIAA Journal* 18.10 (1980), pp. 1213–1220. DOI: 10.2514/3.50873. eprint: https://doi.org/10.2514/3.50873. URL: https://doi.org/10.2514/3.50873.

[32] Donald B. Hanson. "Influence of Propeller Design Parameters on Far-Field Harmonic Noise in Forward Flight". In: *AIAA Journal* 18.11 (1980), pp. 1313–1319. DOI: 10.2514/3.50887. eprint: https://doi.org/10.2514/3.50887. URL: https://doi.org/10.2514/3.50887.

[33] A-21 Aircraft Noise Measure Noise Aviation Emission Modeling. *Prediction Procedure for Near-Field and Far-Field Propeller Noise: SAE AIR 1407*. 400 Commonwealth Drive, Warrendale, PA, United States, 1977. DOI: 10.4271/AIR1407.

[34] F. Farassat. *Derivation of Formulations 1 and 1A of Farassat*. Ed. by National Aeronautics and Space Administration. Washington, D.C., United States, 2007. URL: https://ntrs.nasa.gov/citations/20070010579.

[35] Harvey H. Hubbard. *Aeroacoustics of Flight Vehicles: Theory and Practice*. Tech. rep. NASA-RP-1258-VOL-1. 1991. URL: https://ntrs.nasa.gov/citations/19920001380.

[36] Deepak C. Akiwate et al. "On the balance between the tonal and broadband noise of isolated propellers". In: *International Journal of Aeroacoustics* 23.1-2 (2024), pp. 122–153. ISSN: 1475-472X. DOI: 10.1177/1475472X231225631.

[37] TU Braunschweig, Institut für Flugführung.

[38] Martin Siggel et al. "TiGL: An Open Source Computational Geometry Library for Parametric Aircraft Design". In: *Mathematics in Computer Science* (2019). URL: https://elib.dlr.de/124524/.

[39] *Jane's: All the World's Aircraft 2004-2005*. Jane's Information Group, 2004.

[40] Cessna Aircraft Company. *Information Manual: Model 406*. English. Cessna Aircraft Company. Mar. 2020. Issued.

[41] Jan Roskam. *Airplane Design Part V: Component Weight Estimation*. Design, Analysis and Research Corporation (DARcorporation), 2017.

[42] *F 406*. Type-Certificate Data Sheet EASA.A.109. Issue 06. European Union Aviation Safety Safety Agency, Oct. 2021.

[43] GasTurb GmbH. URL: https://www.gasturb.com/.

[44] MT-Propeller Entwicklung GmbH. URL: https://www.mt-propeller.com/.

[45] *PT6A-100 series engines*. Type-Certificate Data Sheet No. IM.E.094. Issue 03. European Union Aviation Safety Safety Agency, Mar. 2023.

[46] OpenStreetMap contributors. *Planet dump retrieved from https://planet.osm.org*. https://www.openstreetmap.org. 2017.

[47] Bundesministerium der Justiz. *Erste Verordnung zur Durchführung des Gesetzes zum Schutz gegen Fluglärm (Verordnung über die Datenerfassung und das Berechnungsverfahren für die Festsetzung von Lärmschutzbereichen - 1. FlugLSV)*. 2008.

[48] M.J.T. Smith. *Aircraft Noise*. Cambridge Aerospace Series, Cambridge University Press, ISBN 0-521-61699-9, 2004.

[49] *Annex 16 to the Convention on International Civil Aviation*. Volume I - Aircraft Noise. International Civil Aviation Organization, 2017.

[50] D. Heimann and G. Gross. "Coupled simulation of meteorological parameters and sound level in a narrow valley". In: *Applied Acoustics* 56.2 (1999), pp. 73–100. ISSN: 0003682X. DOI: 10.1016/S0003-682X(98)00018-8.

[51] Janicke Consulting. *LASPORT: A program system for the calculation of airport-related pollutant emissions and concentrations in the lower atmosphere*. 2023. URL: https://www.janicke.de/en/lasport.html.